INTERLAMINAR FRACTURE TOUGHNESS OF A QUASI-3D COMPOSITE

By

Anthony Wente

A THESIS

Submitted to
Michigan State University
in partial fulfillment of the requirements
for the degree of

Mechanical Engineering — Master of Science

2019

ABSTRACT

INTERLAMINAR FRACTURE TOUGHNESS OF A QUASI-3D COMPOSITE

By

Anthony Wente

Fiber reinforced polymer (FRP) composites are a heavily sought-after material for light-weighting components in next generation vehicles due to their high specific strength and stiffness. Traditional laminates have relatively weak interlaminar strength and are prone to delamination, and this is especially the case when a delamination crack already exists. Quasi-3D (Q3D) braided composites seek to solve this issue by weaving the bias tows around the axial tows of the adjacent (above and below) plies.

The [0°/60°/-60°] UD and Q3D carbon composites are investigated in this study for their relative in-plane isotropy. Mode I and mode II interlaminar fracture toughness tests were conducted on UD and Q3D samples.

In mode I experiments, the samples were continuously loaded to full beam split using the double cantilever beam (DCB) method to obtain the fracture toughness throughout the sample. The Q3D composite shows a large increase in fracture toughness once the crack stabilizes and the interlaminar tows become engaged.

In mode II testing under end-notch flexural (ENF) test conditions, the Q3D composite shows a significant increase in fracture toughness after a pre-crack has formed and the interlaminar tows have been engaged. The 4ENF test also proves to be a good method for creating a mode II resistance curve that could only be achieved through extensive testing through traditional methods.

This thesis is dedicated to my parents for all of their love and support.

ACKNOWLEDGMENTS

I would like to acknowledge my advisor, Dr. Sharon Xiao, for her guidance and support through graduate school. I am also thankful for all of those who taught and helped me with experimental methods. These include, in no particular order, Wu Zhou, Erik Stitt, Xinyu Mao, Shutian Yan, Italo Benedetti, and Royal Ihuaenyi. Without their help, this thesis would not have been possible. I would also like to express my appreciation for Dr. Danielle Zeng and Homa Torab at the Ford Motor Company for their guidance and support throughout this project.

TABLE OF CONTENTS

LIST OF TABLES

LIST OF FIGURES

KEY TO SYMBOLS

UD	Unidirectional
2DW	2 Dimensional Woven
Q3D	Quasi-3 Dimensional Braided
VARTM	Vacuum Assisted Resin Transfer Molding
PTFE	Polytetrafluoroethylene
G_I	Mode I Fracture Toughness
G_{IC}	Mode I Initial Fracture Toughness
G_Q	Mode II Fracture Toughness Tentative Value
G_{II}	Mode II Fracture Toughness
ENF	End Notch Flexure
NPC	No Pre-Crack
PC	Pre-Crack
b	Width
h	Thickness (Mode I) Half Thickness (Mode II)
P	Load
L	Length of Specimen (Mode I) Half Support Span (Mode II)
d	Loading Span
a	Crack Length
a_o	Initial Pre-crack Length
δ	Load Point Extension
4ENF	4 Point End Notch Flexure
ELS	End Load Split

ONF	Over-notched Flexure
L_g	Extensometer Gage Length
A	Cross-sectional Area

Chapter 1: Introduction

The high demand for more fuel efficient vehicles has increased the necessity to use high-specific strength and stiffness materials. This is especially true with the budding electric vehicle divisions in the automotive industry because the range of the vehicles has been an important issue. In this example, there are two ways to increase the range of the vehicle. One would be to make a more efficient powertrain using higher energy density batteries and more efficient motors. Another would be to make the vehicle's chassis, bodywork, and other components lighter. One method for light-weighting is to use the aforementioned high-specific stiffness and strength materials. Carbon-fiber reinforced polymers (CFRPs) have been proven in the aerospace, racing, and sporting industries as a prime example of this type of material. The use of CFRPs currently range from tennis racquets to Formula 1 chassis to commercial jet fuselages. CFRPs have shown time and time again that they can be used when high strength and stiffness coupled with a low mass is paramount.

However, one major issue with CFRPs is the failure mode of delamination under out-of-plane impact loading. This is a major issue in the automotive industry due to high crash-safety standards. In a typical automotive crash, critical composite parts can experience impact loading in the through-thickness direction and cause delamination. If the delamination resistance of the composite can be improved, the composite can have better specific energy absorption properties. A composite with a higher fracture toughness will also have less crack propagation in an event with crack damage. With less damage, the component will maintain a higher stiffness and strength compared to a comparable composite with a lower fracture toughness. This is extremely important for the crash-safety critical components of a vehicle like bumpers, roof headers, and frame rails where CFRPs can make

a big impact in mass savings.

There have been many proposed solutions for increasing the fracture toughness of laminated composites, and two of the most common methods include stitching [6, 7, 8, 9] and z-pinning [8, 9, 10]. In both of these methods, the composite preform is first compiled, and the through-thickness reinforcement is later inserted into the preform. These reinforcements are also typically inserted orthogonal to the fibers in the laminate: purely in the 3-direction respective to the fibers. Stitched composites are manufactured by taking a preform and using a stitching machine to run a needle with a high-strength yarn through the preform [6, 7, 8, 9, 11], where z-pinning takes the preform and inserts small rods made of a metal or composite into the preform [8, 9, 10]. Both of these methods have been shown to improve the mode I and mode II fracture toughness with typical increases in G_{IC} of around 75% [6, 12] with the steady state crack growth resistance, G_{I}, increasing by factor of 2.9-15.7 [12] in stitched composites. Similar increases are found with laminates that are improved by z-pinning with the G_{I} value typically increasing by a magnitude [13, 14, 15]. Z-pins have also increased the mode II fracture toughness, G_{II}, but not by as significant of an amount. Cartie et.al. found a 2-5 factor increase depending on the density and diameter of the pins being used [13].

While stitching and z-pinning may increase the fracture toughness of the composites, it has been found that they also reduce the in-plane properties that make them desirable initially. In a review paper by Mouritz, Leong, and Hersberg, tensile properties can be reduced anywhere from 30% to 45% and compressive properties can be reduced by 5% to 55% due to stitching [11]. The values for the degradation, along with whether or not the properties are actually degraded, largely vary between the papers reviewed; however, the majority of papers show degradation in the in-plane properties. This degradation has been

attributed to fiber damage/breakage and fiber angle spreading due to the insertion of the needle in the stitching process [11]. Z-pinning also experiences fiber angle spread along with resin rich areas around the pin [8, 10, 16]. For thick pins with a 2% pin density in the laminate, Mouritz found that there is a range of 7%-17% decrease in Young's Modulus and typically a 11%-14% decrease in compressive strength depending on the layup sequence [16]. It is also found that tensile strength is typically degraded by 5%-10% and the fatigue performance is reduced [15].

It has been shown by by Kerber et. al. that the use of a z-binder reinforcement improves the fracture toughness of a composite without a great reduction in the in-plane properties [17]. These z-binder fibers are woven into the laminate along with the fibers in the warp direction, and they are woven around each fiber in the fiber in the weft direction. This keeps the reinforcement relatively flat; however, the z-binder reinforcement is still significantly in the 3-direction, reducing the in-plane properties. The authors found that as the amount of z-binders are increased, the flexural properties on the composite decrease. It was also shown that for a 100% increase in fracture toughness, whether mode I or mode II, the blast-induced delamination damage will be reduced by over 50% [17].

Quasi 3-dimensional (Q3D) composites are seeking to increase the fracture toughness of a fiber-reinforced composite without degrading the desirable in-plane properties. Q3D composites differ from other fracture toughness increase mechanisms by not using a through-thickness reinforcement that is orthogonal to the fibers. Q3D differs from the previously mentioned z-binder reinforcement because the through thickness reinforcement in not added to an existing preform, and one reinforcement is not woven through all layers. Instead, the fiber tows are braided in such a way that instead of each tow being constrained to a single layer, it is also braided into the adjacent layers from which it originates. In the case of

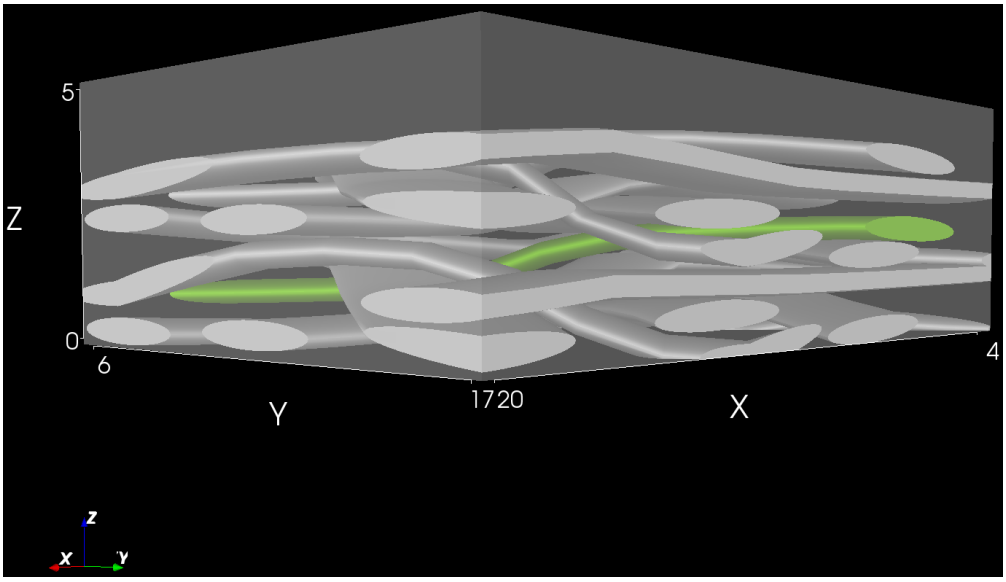

Figure 1.1: Q3D unit cell with the bias tow that is braided between the layers highlighted [1]

the triaxially braided composites being investigated in this study, the bias tows are braided in into the layers adjacent to their originating layer, and the axial tows remain straight within their respective layer. This keeps the through-thickness reinforcement used in a Q3D preform flatter than that used in the z-binder composite. Furthermore, the through-thickness reinforcement in a Q3D composite consists of the bias tows with no additional reinforcement needed that displaces the fibers in the pre-existing preform where the z-binder introduces new binder tows.

Figure 1.1 highlights a tow that bridges this interlaminar gap. To give a more specific example, a bias tow in the third layer of a composite will not only be braided around the axial tows of the third layer, but it will also be braided around the axial tows of the second and fourth layers as well. These bias tows then bridge the gap between layers such that fiber breakage is required for crack propagation instead of simply matrix failure. When a preform of a Q3D structure is created, there are not individual layers as with traditional laminated composites. Instead, there is a single preform where every layer is now braided together.

More information about Q3D composites can be found in US Patent US009273933 [18].

Because the bias tows are only braided into the adjacent layers and not through the full laminate, they remain relatively flat. There is also no post-processing of the preform required with needle or pin insertion, so there is no extra fiber damage, fiber spreading, or resin-rich areas that form. This also reduces the handling of the carbon fiber because there is one less step as opposed to other traditional delamination resistance mechanisms. Rosario and Liu found that the Q3D architecture for biaxially woven composites have competitive in-plane properties to its laminated counterpart while also having increased impact properties [19]. Wu Zhou tested the in-plane tensile properties of the [0°/60°/-60°] Q3D composite in his PhD thesis and found that in the axial direction, the Q3D tensile strength exhibits between 5-10% degradation compared to the unidirectional (UD) laminate, but the Q3D and traditional woven (2DW) laminates have comparable tensile strengths. It is also found that transverse to the axial direction, all three composites have nearly identical tensile strengths. As for the tensile modulus, the UD, 2DW, and Q3D laminates were all within 5-10% of each other [2]. Many authors have also investigated the effects of the Q3D composites with respect to their energy absorption and damage resistance due to out-of-plane impact and have found that the Q3D structures will absorb a similar amount of energy with a smaller damage area [2, 19, 20] and have lower displacement, approximately the same force, and a higher bending stiffness compared to UD and 2DW [20]. A study performed by Bayraktar, et al showed that a Q3D composite will have a higher specific energy absorption in terms of weight for energy absorbing structures in automotive vehicles when constant cross section composite and steel beams are compared [21].

This thesis investigates Q3D composites and the effect that the bias tows bridging the ply interface have on the mode I and mode II fracture toughness. Attention is especially paid

to the steady state growth of the crack as opposed to simply the initial values to determine the relationship between the crack length and the fracture toughness in both the UD and Q3D composites.

Chapter 2: Manufacturing

2.1 Preforming

In this study, preforms are created in two different fashions: using a braiding machine and hand braiding. The braiding machine is used to create the preforms for the in-plane and hat section testing, but hand braiding is required for fracture toughness testing. The fiber used with the braiding machine is DowAksa 24k A-42 carbon fiber, and the fiber used during hand-braiding is DowAksa 12k A-42 carbon fiber. Figure 2.1 compares the handwoven preforms for each of the UD, 2DW, and Q3D preforms. It also shows a schematic for a comparison of the number and relative thickness of the layers within the preform.

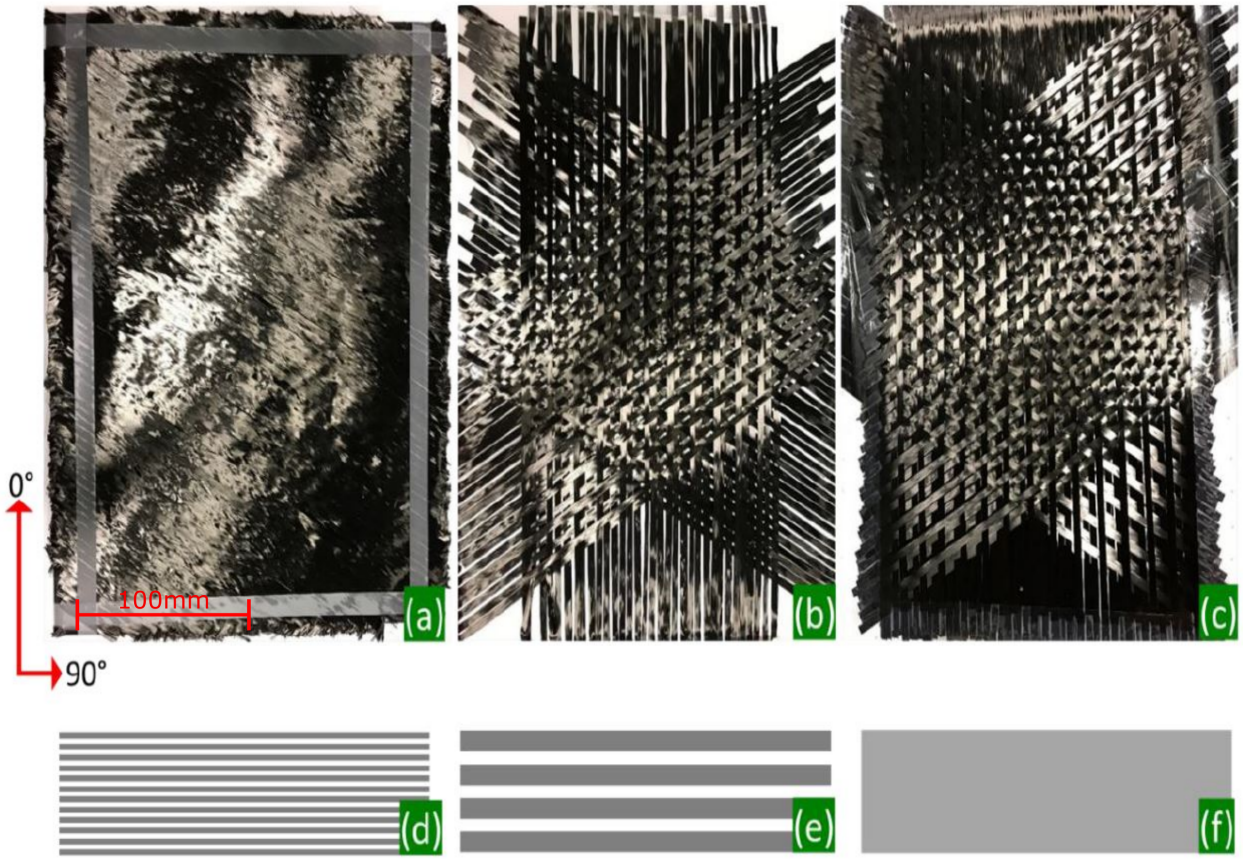

Figure 2.1: Comparison of handwoven architecture [2].

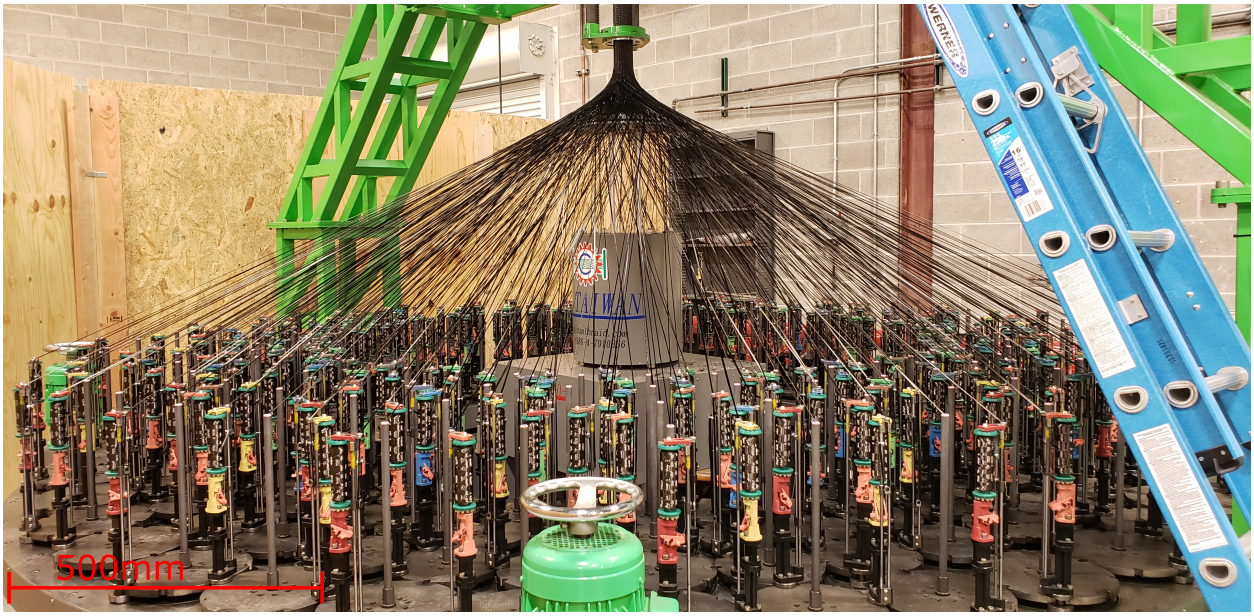

Figure 2.2: Braiding machine used to create preforms used in this thesis

2.1.1 Braiding Machine

The triaxially braided Q3D structure is made by using a large braiding machine with 480 bobbins. 120 of these bobbins are for the axial tows while the other 360 are for the bias tows. Figure 2.2 shows the machine used to make the preforms. In this figure, the carriers and the bobbins holding the bias tows can clearly be seen along with the beginning of the braided tube. The axial tows can also be seen coming out of the long, slender rod in the center of the base at which the carriers rotate. This type of preform is required to be braided into a tube because it is triaxial in nature. The machine works by pulling up the braided tube through four rollers. This is referred to as the uptake. As it is being pulled up, the axial tows remain straight and taught while the bias tows are being maneuvered around them. By changing the speed at which the carriers holding the bias tows are moving along with the speed of the uptake, the braided angle can be changed.

Once a sufficient length of tube is braided, it can be cut from the machine to be infused

Figure 2.3: Braided Q3D tube braided from machine

or laid up. It can be kept as a tube, but for this study, the tube is cut length-wise to create a flat preform. Figure 2.3 and 2.4 show this Q3D preform as a tube and flat preform, respectively. More information about the manufacture of a triaxially braided Q3D composite can be found in the aforementioned patent [18].

2.1.2 Hand Braiding

When investigating the fracture toughness of a composite, a pre-crack is required in the end of the specimen. The machine being used to braid the Q3D architecture does not have a method for adding a pre-crack, thus the fracture toughness samples must be hand braided. Because the hand braiding of the pre-forms is extremely labor intensive and time consuming, a single

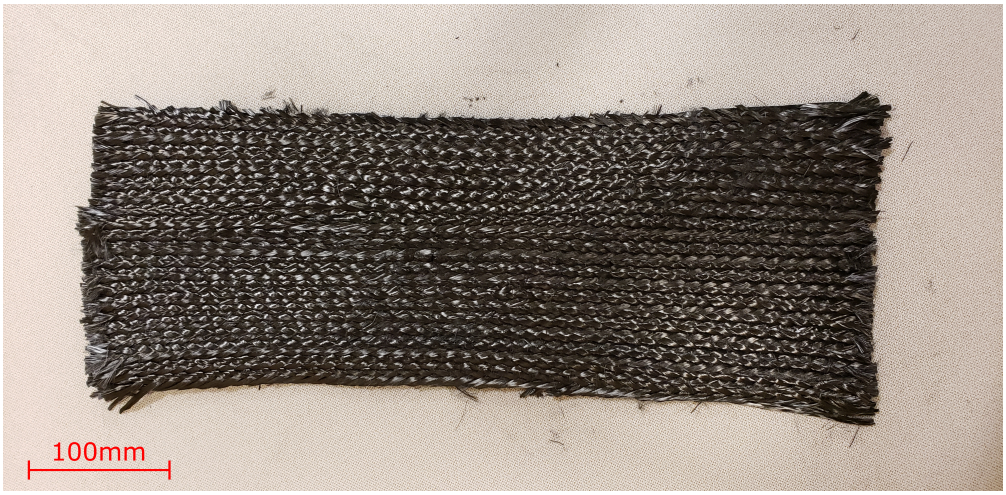

Figure 2.4: Flat Q3D preform crease by cutting tube length-wise

[0°/60°/-60°] layer of the investigated architecture is used symmetrically on each side of the crack surface. If the laminate is too thin, failure can occur at the outsides of the laminate or the arms in mode I testing or the outer skins will fail before crack propagation during mode II. To counteract this, the thickness can be built up using a unidirectional or textile material stacked on each side of the desired preform until the optimal thickness is achieved [17]. To achieve this higher thickness, five layers of A&P Technologies triaxially braided [0°/60°/-60°] carbon fiber is used on either side of the studied layers. This thickness is required such that delamination is the failure mechanism during the experiments as opposed to in-plane fiber or matrix failure. It has been shown in previous works that a sufficiently thin PTFE (Teflon®) or polyimide (Kapton®) film is sufficient for creating the necessary pre-crack in fracture toughness testing [17, 22, 23, 24]. For this study, a 0.001 inch thin (Kapton®) film is used to create the pre-crack between the two layers of the studied architecture. Because the Q3D architecture has the through-thickness tows throughout the preform, one end was braided such that there were not any of these tows for approximately 65mm such that the film could be inserted. Figure 2.5 shows a schematic of the stacking sequence used to create

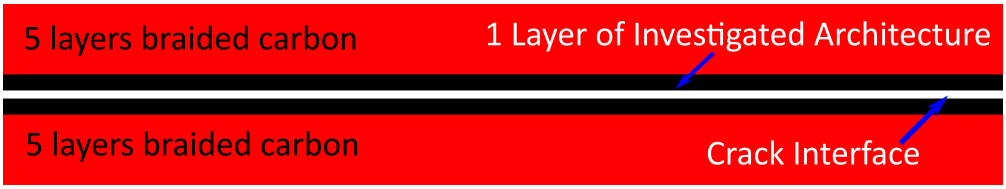

Figure 2.5: Schematic showing layers of laminates for fracture toughness testing with the tested architectures in the middle and the commercially available triaxially braided composite on the outer layers.

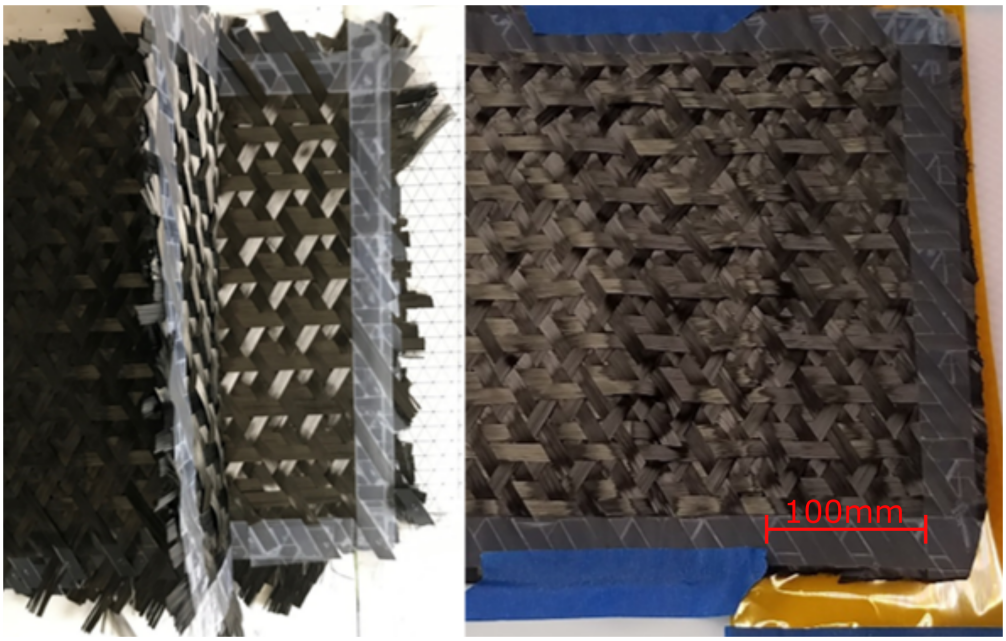

Figure 2.6: Images showing how the pre-crack is generated in the Q3D composite. The orange, polyimide film can be seen in the cured laminate.

the fracture toughness laminates. Figure 2.6 shows how one end of the preform does not have the through-thickness tows, and the film is inserted to create the pre-crack during infusion.

2.2 Infusion

The preforms are infused with API SC-15 toughened epoxy through vacuum-assisted resin transfer molding (VARTM). The in-plane and fracture toughness specimens are manufactured on a flat, aluminum caul plate, or tool, that is sanded and prepped after every use. The preform is placed straight onto the caul plate, and a layer of peel ply is placed on top of the preform to separate the infusion media from the preform such that is does not stick. The

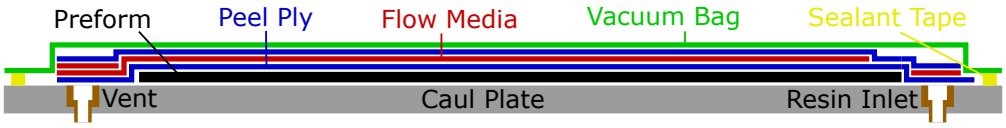

Figure 2.7: Schematic of infusion showing the different layers of consumables

infusion media is then added from the resin inlet to the vent with approximately a 20mm break in it at the end of the preform. This is to force the resin front to slow such that it diffuses fully through the preform. Another layer of peel ply is added on top of the infusion media to dull the sharp edges and protect the bag from popping under vacuum. Small pieces of breather can be added over the resin inlet and vent to ensure that the bag does not create a seal at these two ports. The bag is then carefully stuck to the caul plate. Great care is taken to ensure there are no wrinkles in the bag at the sealant tape and no leaks form once vacuum is applied. Figure 2.7 shows a schematic of the different layers within the bag during an infusion. Once fully assembled, the resin inlet is clamped and vacuum is pulled. Vacuum is then pulled at 28inHg, measured in the catch pot. Once this full pressure is reached, the pump is turned off for 15 minutes, and the pressure is monitored. If there is no discernible pressure drop in the analog gauge after those 15 minutes, the bag is deemed to be leak free. The vacuum will then be turned back on for 15 minutes to boil any residual moisture in the bag and preform and suck it out. If this is not done, this moisture could be trapped within the resin, causing voids. During this time, the epoxy resin is mixed and degassed for 10-15 minutes in a vacuum chamber. Once the resin is degassed, the tube at the resin inlet is placed in the resin pot, and the clamp is released. The infusion process begins, and this will take typically 30-60 minutes depending on the architecture and size of the preform. Three steps of the infusion process are shown in figure 2.8. Once the preform has been fully infused, it is placed in a convection oven to cure. There is a joint in the tubing between the

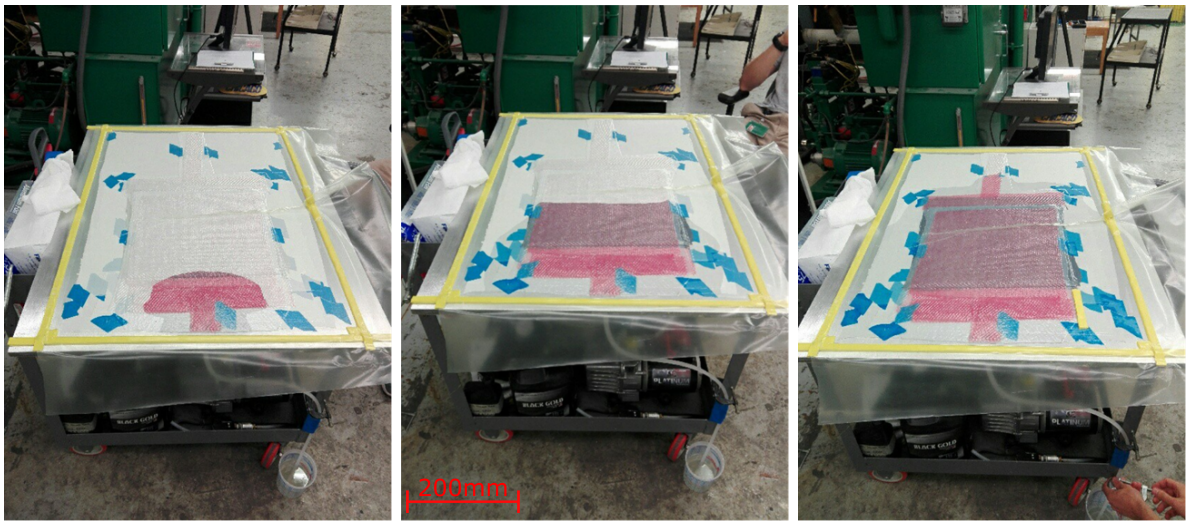

Figure 2.8: Infusion process at three different points

catch pot and caul plate that allows the tool to be placed into the oven and still be under vacuum during the full cure cycle. The laminate is then vitrified at 60°C for two hours, and then it is post-cured at 94°C for four hours.

2.3 Volume Fraction Determination

The volume fractions are obtained initially by weighing the dry fiber preform before resin infusion then dividing that mass by the mass measured after the laminate is cured to obtain a weight fraction. The densities of the resin and the fibers are then used to get a volume fraction. The weight of the polyamide film is taken to account in this measurement, and the values are confirmed by sulfuric acid digestion following the ASTM standard D3171-15 [25]. Figure 2.9 shows the setup for this procedure for the acid digestion. Small pieces of the laminate are weighed to the nearest milligram, and then placed in the heated acid inside of a fume hood to digest the matrix. Once the matrix has been digested, the mixture is poured into the funnel to get rid of the acid and matrix mixture. The fibers are sprayed with distilled water and then acetone to remove all of the acid. Once all of the acid is

Figure 2.9: Setup for acid digestion of the matrix to determine fiber volume fraction

Figure 2.10: Carbon fibers after acid digestion and oven drying

removed, the fibers are oven dried and weighed again. Figure 2.10 shows the carbon fibers after oven drying. The weight of the dry fibers divided by the weight of the original laminate will give the weight fraction of the fibers. Comparing the weight fraction from acid digestion to the weight fraction from weighing the preform before infusion and the laminate after infusion yields the same results within certainty. Table 2.1 shows the volume fractions for

Table 2.1: Volume Fractions [%]

Tests	$\mathbf{V_f}$
Fracture Toughness	60.0±0.5
Hat Section	55.5±0.5
In-Plane	55.5±0.5

the laminates in this study. The reason for the fracture toughness samples having a higher volume fraction is likely due to the tighter weave of the commercial fabric used to build up the thickness.

Chapter 3: Fracture Toughness

3.1 Background

Fracture toughness is an important property of laminated composite materials due to their relative ease to delaminate. Laminated composites are made of layers, or plies, of unidirectional or woven, textile composites within a matrix. In this study a thermoset epoxy-resin polymer is used as the matrix. The fibers have a modulus of 240 GPa and a tensile strength of 4200 MPa [2]. In contrast, the SC-15 toughened epoxy has a modulus of 2.62 GPa and tensile strength of 56.4 MPa [26]. The fibers have a stiffness and strength nearly two magnitudes above that of the matrix. In a traditional laminate, the layers are only separated by this relatively weak matrix. The methods for increasing the fracture toughness for a composite typically consist of either increasing the fracture toughness of the matrix or mechanical interlocking from stitching, z-pinning, or Q3D braiding. The SC-15 epoxy-resin used in this study is already rubber toughened, thus improvements seen by the Q3D structure will not be as prominent as they would in a composite where the resin is not toughened.

There are three modes when looking at fracture toughness as shown in figure 3.1. The two studied in this thesis are mode I: opening and mode II: in-plane shear. The mode II in-plane shear is especially relevant for the out-of-plane impact seen in crash scenarios for automotive vehicles.

In this work, only mode I and mode II fracture toughness is investigated because these are the two commonly seen in the real world. Mode III is also difficult to test for, and there is not a currently accepted standard for it as of the time this thesis is written. In mode I fracture toughness, the toughing mechanism of the interlaminar fiber will have a large effect

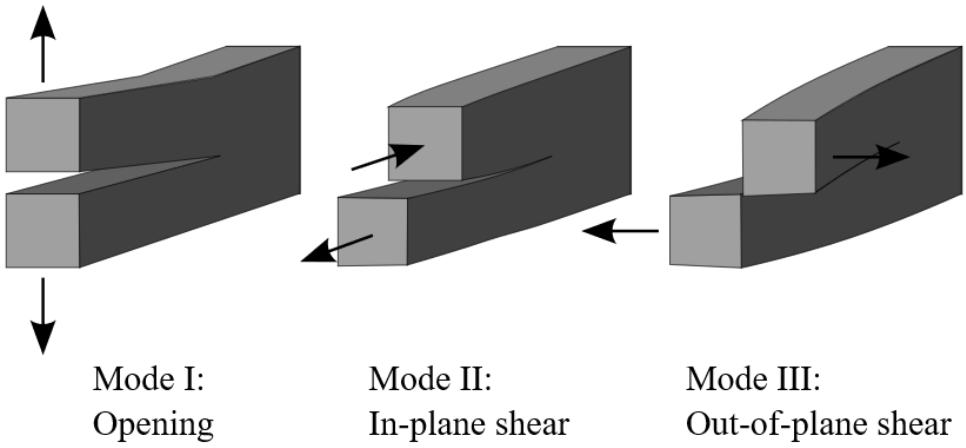

Figure 3.1: The 3 different fracture modes

due to the requirement for the tow to break. In mode II, the interlaminar fiber tow will require the crack to propagate around the tow, but not necessarily break it.

3.2 Mode I

3.2.1 Experiment

The mode I experiments follow the testing basis given by ASTM standard D5528 [3]. The two methods for loading the specimen are piano hinges and loading blocks. Piano hinges were first implored, but the large deformation required to fully split the sample made it such that the beam came into contact with the grips. For this reason, loading blocks are used with a steel wire through the block and into the grips. This allows for sufficient space between the sample and the grips so there is no interaction. Similar to previous studies, the side of the specimen is painted white, and markings are made every 5mm [22]. The first 20mm is marked every 1mm. This is so that the initial crack propagation can be better visualized because the initial fracture toughness, G_{IC}, is defined by the first 1mm of crack growth. It is also very difficult to determine where the manufactured crack tip is, and precise marking

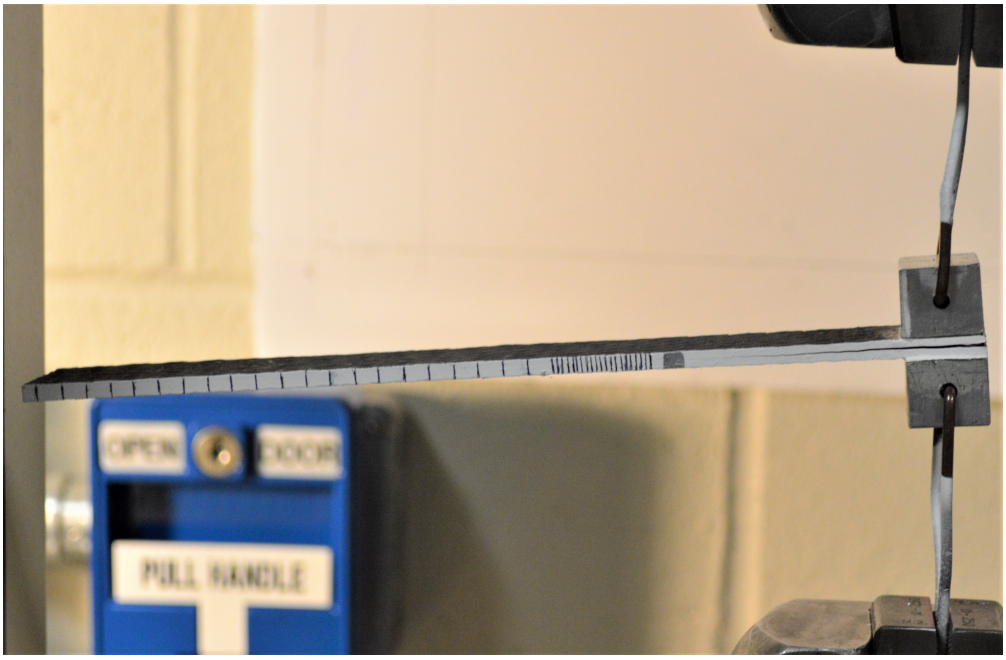

Figure 3.2: Mode I specimen at beginning of test showing the wires for loading and markings on side on specimen

near the estimated crack tip allows for accurate adjustment after the test. An example of a specimen during the test is shown in figure 3.2. Using a camera to record the crack length during the test has been shown to be an effective method for measuring the crack propagation during the test [17]. Using the camera to record the experiment allows the test to be run continuously without the need to unload after crack growth. This is useful for saving the amount of time required to run a test, accuracy of measuring the location of the crack tip without the possibility of damaging the specimen further, and it reduced the risk of loading history causing artifacts within the data. The camera used records the experiment by acquiring images at a rate of 1 $\frac{\text{image}}{\text{second}}$ to match the sampling rate of the machine at 1 Hz. The setup of the experiment with the camera and light source is shown in figure 3.3. The machine used for this and all fracture toughness tests is the MTS Insight Electromechanical test frame. In these experiments, the crosshead speed is set at 5 $\frac{\text{mm}}{\text{min}}$. The test is run until the crack propagates completely through the specimen, and the specimen is split into two.

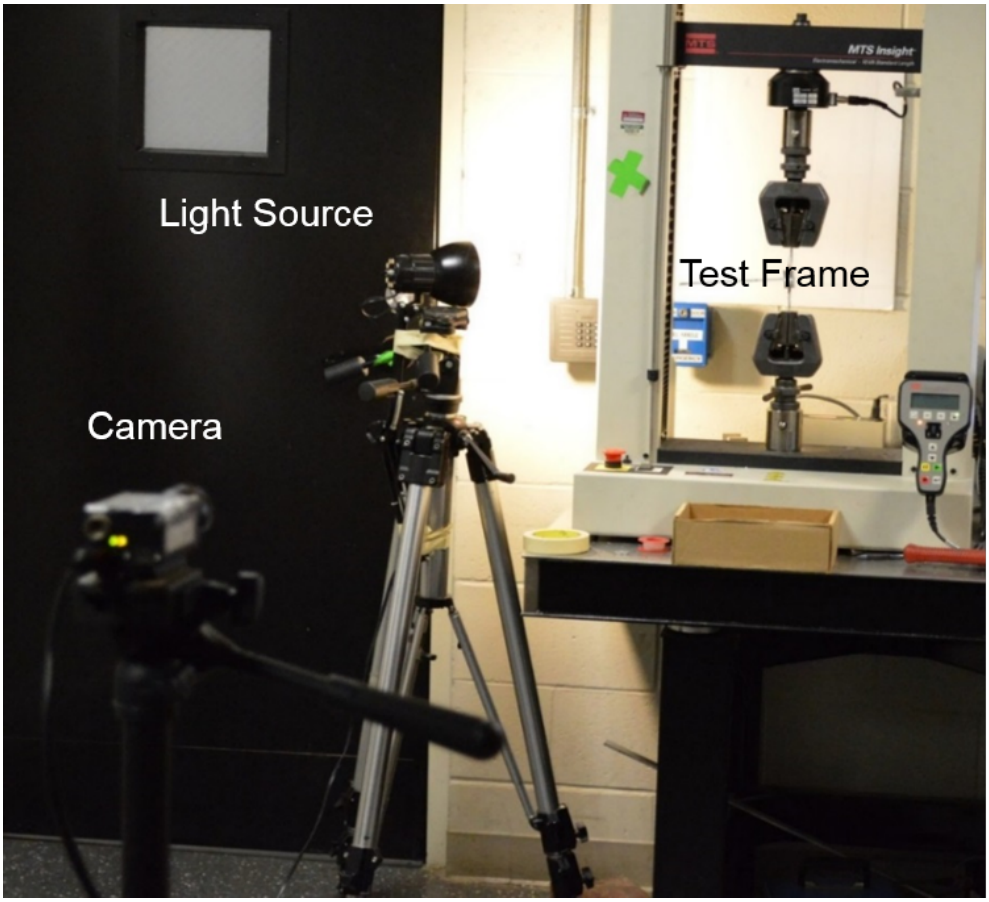

Figure 3.3: Test setup for mode I experiment with camera and light source

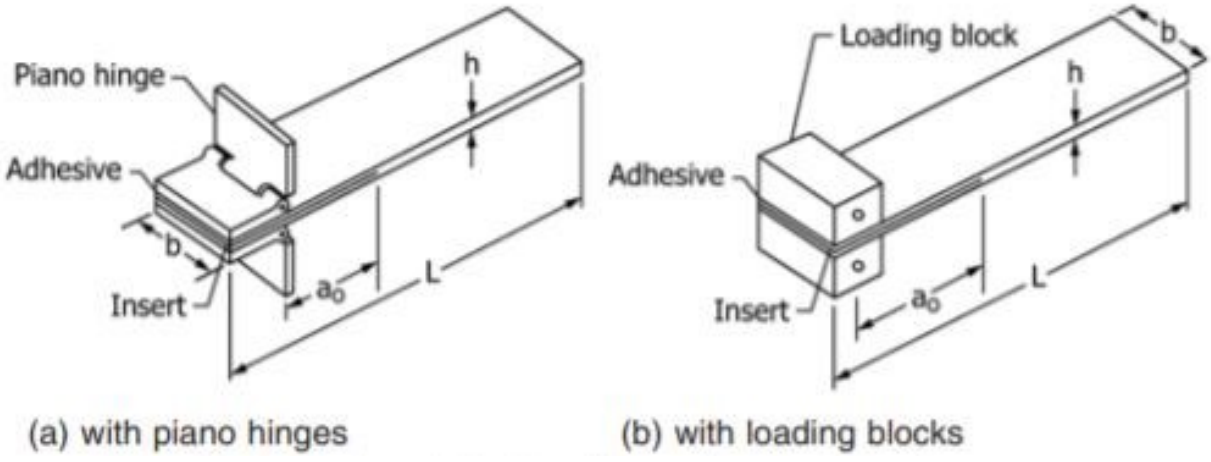

Figure 3.4: Critical dimensions for DCB test [3]

Table 3.1: Mode I Sample Dimensions [mm]

Specimen	**b**	**h**	$\mathbf{a_o}$
UD1	25.4	3.528	56.1
UD2	25.1	3.606	54.1
2DW1	25.9	3.554	56.3
2DW2	25.8	3.564	55.0
Q3D1	25.5	3.620	61.8
Q3D2	25.5	3.480	59.9

Table 3.1 shows the dimensions of each mode I sample with the corresponding dimensions showing in figure 3.4.

3.2.2 Results

For mode I, the fracture toughness is calculated as a function of load, extension, crack length, and specimen geometry. In this study, the modified beam theory (MBT) is used to calculate the G_I value. The initial fracture toughness value, G_{IC}, is calculated at the point when the crack has propagated by 1mm, and this is determined by using the images acquired during the test. Equation 3.1 is used for determining the G_I value.

$$G_{\mathrm{I}} = F\frac{3P\delta}{2B\left(|\Delta| + a\right)} \tag{3.1}$$

In this equation, F is an inclusion factor that takes into account how the specimen geometry is changing during the test. Equation 3.2 shows how the inclusion factor is calculated, and figure 3.5 shows a representation of the variables used in calculating the G_{I} value. The rotation correction factor, Δ, is determined by performing a linear regression on a plot of the cube root of compliance, $C^{1/3}$, as a function of the delamination length, a. The compliance,

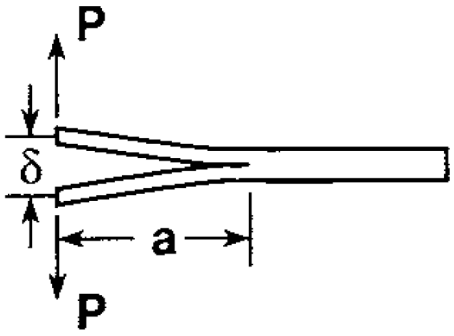

(a) Mode I fracture toughness

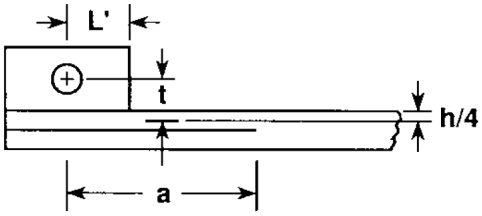

(b) Inclusion factor, F

Figure 3.5: Representation for nomenclature in mode I fracture toughness calculations from ASTMD5528 [3].

Table 3.2: Mode I Averages

	UD	**2DW**	**Q3D**
$G_{\mathrm{IC}}\left[\frac{\mathrm{J}}{\mathrm{m}^2}\right]$	563.6	564.1	466.3
$G_{\mathrm{I}}\left[\frac{\mathrm{J}}{\mathrm{m}^2}\right]$	732.8	730.4	884.7
Energy [J]	3.345	3.756	4.994

Table 3.3: Q3D Mode I Architecture Advantages [%]

	UD	**2DW**
G_{IC}	-17.3	-17.3
G_{I}	20.7	21.1
Energy	49.3	32.9

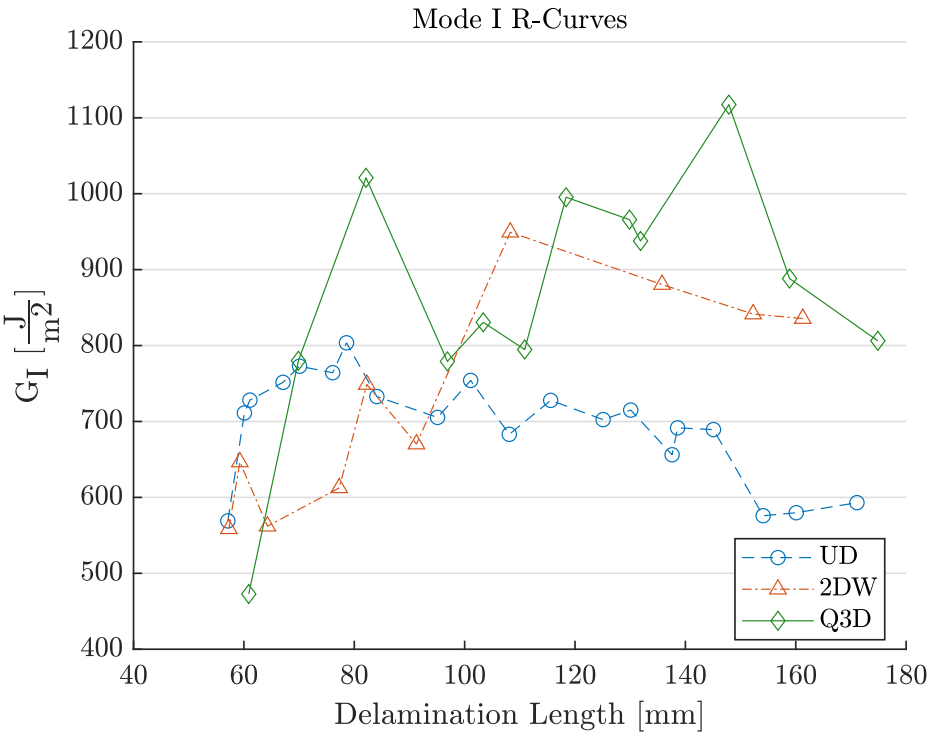

Figure 3.6: R-Curve comparison for all architectures.

C, is defined as $\frac{\delta}{P}$. Δ is then found to be the x-intercept of the linear regression.

$$F = 1 - \frac{3}{10}\left(\frac{\delta}{a}\right)^2 - \frac{3}{2}\left(\frac{\delta h}{a^2}\right) \tag{3.2}$$

Tables 3.2 and 3.3 show the average mode I values for each architecture and the percentage difference between them. It can be seen that the Q3D structure has a lower G_{IC} value, but a larger G_{I} value. This is due to difficulties in creating the pre-crack in the Q3D structure because of the through-thickness tows. The leading edge of the film can wrinkle, causing a stress concentration at the crack tip and a lower G_{IC} value. It can be seen by the resistance curves shown in figure 3.6 that the G_{I} value increases quickly beyond this initial value. More R-curves for each of the fiber architectures are shown in the appendix.

Along with the fracture toughness values, the energy required to fully split the sample

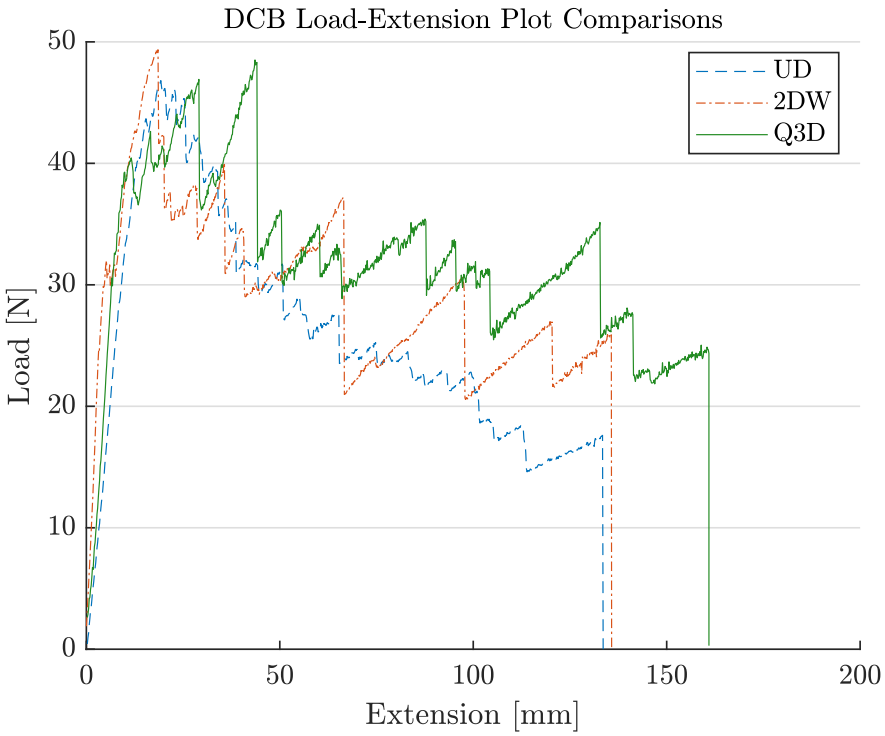

Figure 3.7: Comparison of load-displacement curves for all architectures.

is reported. Each sample has the same length from the crack tip to the free end, so these energy absorption values can be properly compared. This value gives a better comparison of the delamination resistance of each of the material architectures because the amount of crack propagation and the lower initial values have less of an effect. Looking at a comparison of typical load-displacement curves for each of the architectures in figure 3.7, it is seen that it takes more extension for the 2DW to fully split compared to the UD sample. The 2DW will also hold a higher load throughout the experiment, so it would have been expected to have a higher G_{I} value, but this is not the case. This is due to the 2DW having lower fracture toughness values compared to UD initially, but they increase as the crack propagates. The crack also propagates in a stick-slip fashion for the 2DW causing it to have fewer G_{I} values to report, thus lowering its average. The same can be said about the Q3D structure with the larger amount of low G_{I} values initially, but fewer values as the crack propagates and the

Figure 3.8: Fiber bridging crack gap of Q3D specimen.

fracture toughness increases. The energy absorption takes this into account and allows for a better comparison to be made. The Q3D also has a larger increase in energy absorption compared to both the UD and 2DW than it does in fracture toughness.

The Q3D has a more pronounced stick-slip condition compared to the 2DW, and this is due to the interlaminar tows in the Q3D composite bridging the crack interface. The introduction of these tow requires fiber breakage for the crack to propagate, where the UD and 2DW simply require matrix failure. These tows support more load and require a larger crosshead extension before failure. Figure 3.8 shows the interlaminar tow clearly bridging the gap in the middle of a mode I experiment. After failure of this interlaminar tow, the crack will propagate until it reaches the next tow, and crack propagation will cease. At this point, the load will begin to rise again until the next tow breaks. The interlaminar tows are

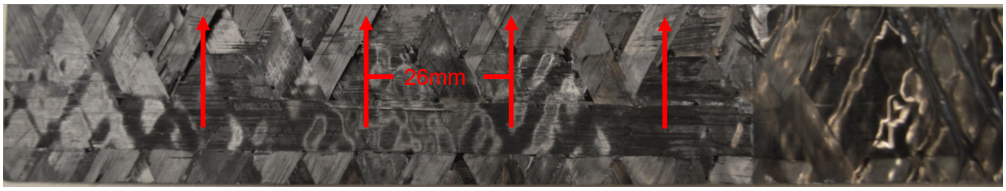

Figure 3.9: Crack interface of Q3D specimen after DCB test. The 26mm spacing of the broken interlaminar tows can be seen.

spaced out by 26mm as shown in figure 3.9. Looking at the resistance curve for the Q3D architecture, it is seen that fracture toughness values are given for crack lengths spacing approximately 26mm as well. The points for the resistance curve correspond to the points immediately before crack propagation that correspond to the max load.

3.3 Mode II

3.3.1 Background

The current standard for measure the mode II fracture toughness of a material is to perform a 3-point end notch flexural (ENF) test. This method gives consistent results, but it only gives a fracture toughness value for one crack length. Furthermore, two tests must be conducted on the same specimen such that a fracture toughness from the blunt crack tip manufactured by the film and the sharp crack tip generated by shear induced crack propagation can be compared. If an R-Curve is desired, multiple tests must be conducted with different initial crack lengths. This can be tedious and also allows opportunity for error and loading history effects. If an R-curve is desired, another test is required and is investigated later in this study.

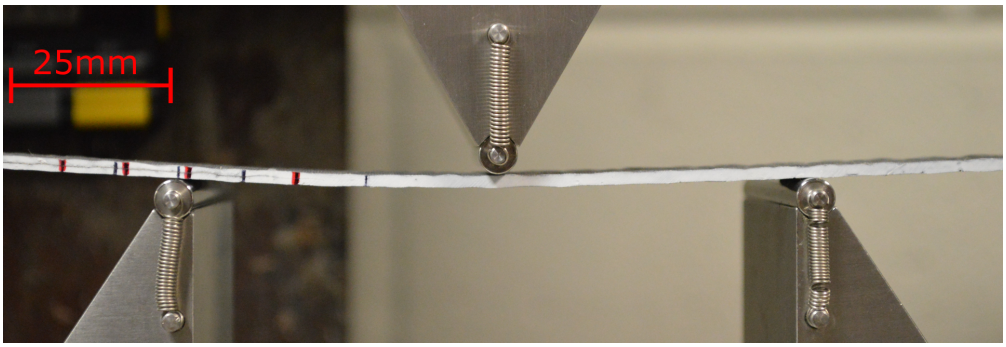

Figure 3.10: ENF specimen during test

3.3.2 3ENF

3.3.2.1 Experiment

Experiments for mode II fracture toughness follow the 3ENF test outlined in ASTM standard D7905 [4]. As with the mode I samples, the sides are painted white such that the crack and the compliance calibration markings can be seen more easily. This is shown in figure 3.10. Crosshead speed during the test is 0.5mm/min.

Compliance calibration is done at 3 initial crack lengths of 20mm, 30mm, and 40mm. For the 20mm and 40mm crack lengths, the test is stopped at half of P_{crit}, where P_{crit} is the load required for crack propagation. For the 30mm crack length test, the test is run until crack propagation and a significant load drop is achieved. The P_{crit} value is determined experimentally for each crack length. Table 3.4 shows the dimensions of each of the mode II samples.

3.3.2.2 Results

The mode II tests have two different tests conditions: no pre-crack (NPC) and pre-crack (PC). For the NPC condition, the initial delamination for the NPC test is simply the manufactured pre-crack, where the initial delamination for the PC test includes crack propagation

Table 3.4: Mode II Sample Dimensions [mm]

Specimen	b	h
UD1	25.2	1.790
UD2	25.3	1.766
2DW1	25.0	1.729
2DW2	24.8	1.778
2DW3	25.4	1.724
Q3D1	24.6	1.814
Q3D2	25.4	1.837

(a) NPC

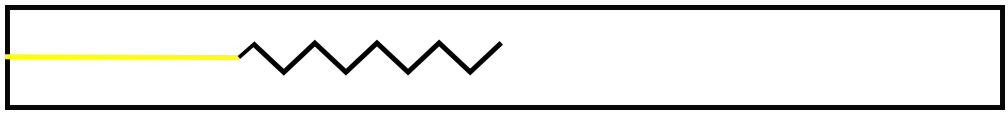

(b) PC

Figure 3.11: Specimen pre-crack conditions for NPC and PC

beyond this point as shown in figure 3.11.

The ENF test used for mode II fracture toughness calculation does not give stable crack growth, and thus, only one G_{II} value can be calculated for a single test. Once crack propagation begins, the delamination rapidly expands until it reaches the loading roller. The fracture toughness is calculated as a function of the initial crack length, max load, specimen width, and compliance calibration curve slope as shown in equation 3.3.

$$G_{\text{Q}} = \frac{3mP_{Max}^2 a_0^2}{2b} \tag{3.3}$$

The compliance calibration curve slope is obtained by the linear regression of the compliance vs crack length cubed plot. The compliance for a particular crack length is taken from the range of 90N to the $\frac{P_{\text{crit}}}{2}$ value that was determined. This is done such that any non-linearities

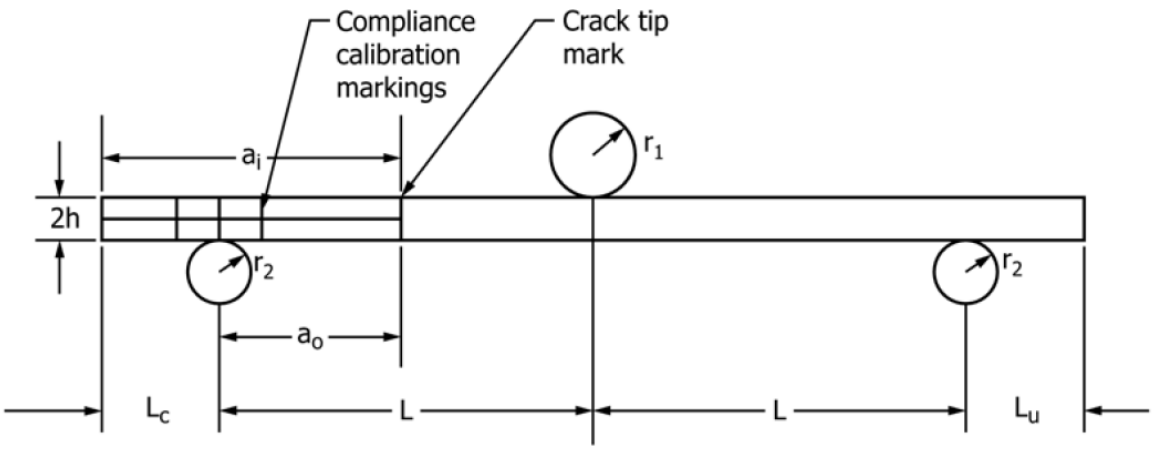

Figure 3.12: Representation of nomenclature for ENF test from ASTMD7905 [4].

from the fixture at the beginning of the test and any non-linearities from the laminate at higher loads are not influencing the compliance.

For a pictorial representation of the variables used for calculating G_{Q}, figure 3.12 can be referenced. G_{Q} can be considered to be the G_{II} value for the sample only when equation 3.4 is satisfied. If it is not satisfied, then the test must be redone to obtain a G_{II} value.

$$15 \leq \frac{100\left(P_i a_i\right)^2}{\left(P_{\mathrm{Max}} a_0\right)^2} \leq 35; \quad i = 1, 2 \tag{3.4}$$

P_{i} and a_{i} in this equation are the $\frac{P_{\mathrm{crit}}}{2}$ and crack length values used in each compliance calibration test.

As with the mode I tests, Q3D has a higher fracture toughness after initial crack propagation, but a lower value when the crack tip is manufactured from the film. The Q3D sees a higher increase in G_{II} versus that 2DW and UD compared to the increase in G_{I}. The Q3D architecture shows nearly a 47% increase in mode II fracture toughness compared to the UD and an 18% over the 2DW architecture. The G_{II} values and percent difference are shown in tables 3.5 and 3.6, respectively.

Table 3.5: Mode II Averages $\left[\frac{J}{m^2}\right]$

	UD	**2DW**	**Q3D**
NPC	644.5	502.2	613.8
PC	559.5	696.1	824.3

Table 3.6: Q3D Mode II Architecture Advantages [%]

	UD	**2DW**
NPC	-4.8	22.2
PC	47.3	18.4

Similar to the mode I DCB test, the load-displacement plots for the PC mode II tests in figure 3.13 show that the Q3D architecture requires a larger load and extension before crack propagation. The PC plots are shown because they give a better representation of the effect that the Q3D architecture has on fracture toughness. The NPC test does not initially engage the interlaminar tow that increases the fracture toughness for the Q3D composite, and as with the mode I test, the issue with manufacturing the pre-crack for the Q3D structure also gives unrepresentative results. The larger load and extension required for Q3D shows that in mode II testing, the Q3D architecture will have a larger energy absorption than UD or 2DW. More plots for each architecture are shown in the appendix.

3.3.3 4ENF

3.3.3.1 Background

While the ENF test shows that the Q3D architecture has an advantage, it may not show everything. As it is seen in the mode I tests, the Q3D laminate has the largest advantage during steady-state crack growth. With the ENF test, steady-state crack growth is not achievable because of the inherent unsteadiness of the crack.

There have been a few proposals tested to achieve the steady-state crack growth. Some

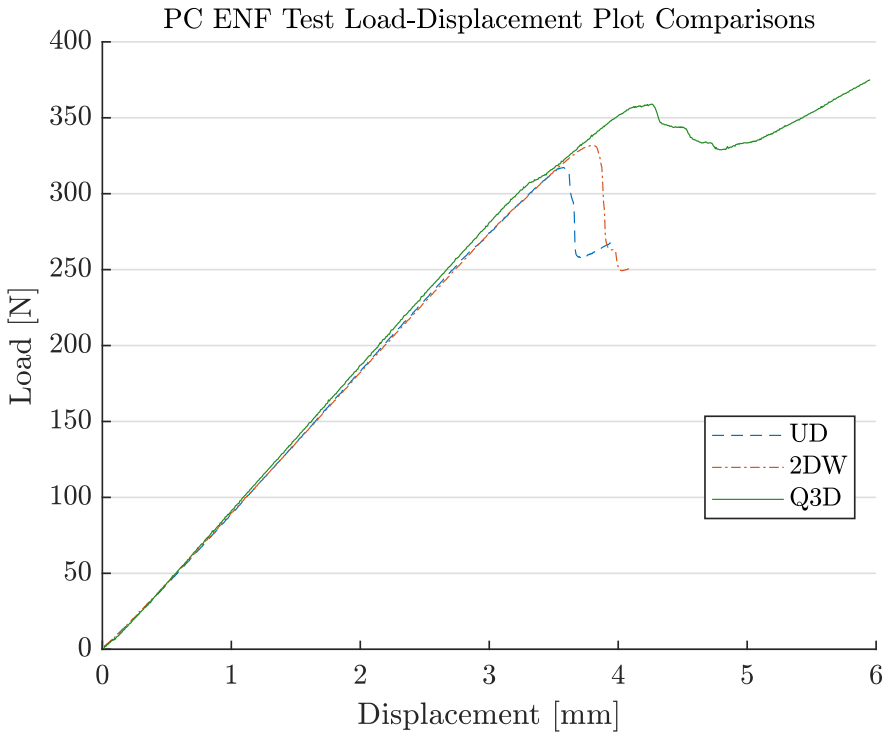

Figure 3.13: ENF test load-displacement curve comparisons for three different architectures during the PC test

of these include the end-loaded split (ELS) test, stabilized ENF, over-notched flexure (ONF) test, and 4ENF. Of these tests, the 4ENF test proved to be the most promising because it produced stable crack growth while also being a relatively simple experiment [24, 27, 28]. Figure 3.14 shows why 3ENF is unstable while 4ENF is stable by using moment diagrams. As the crack grows in the ENF test, it propagates into regions of higher moment, thus causing the crack propagation to continue. However, with the 4ENF test, the crack remains in an area of constant moment and maintains stable crack growth. As the crack grows, the load will drop slightly, decreasing the moment. With the decrease in moment, the crack will cease to propagate until the load increase back to where crack propagation occurred initially. In theory, this will create a load-displacement diagram with a nearly horizontal line after peak loading. Due to issues in manufacturing, friction, and non-ideal loading conditions, this is

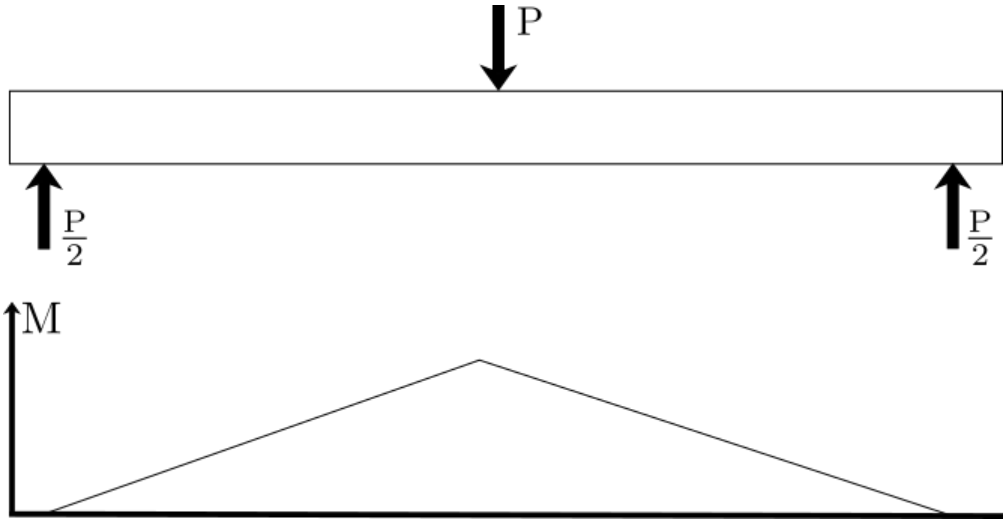

(a) 3 point bend

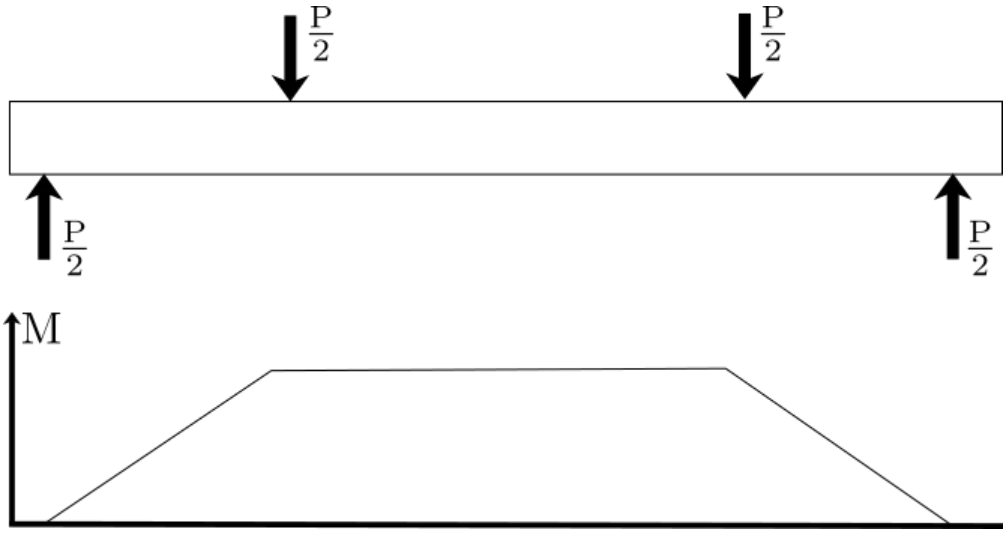

(b) 4 point bend

Figure 3.14: 3 point and 4 point bend moment diagrams

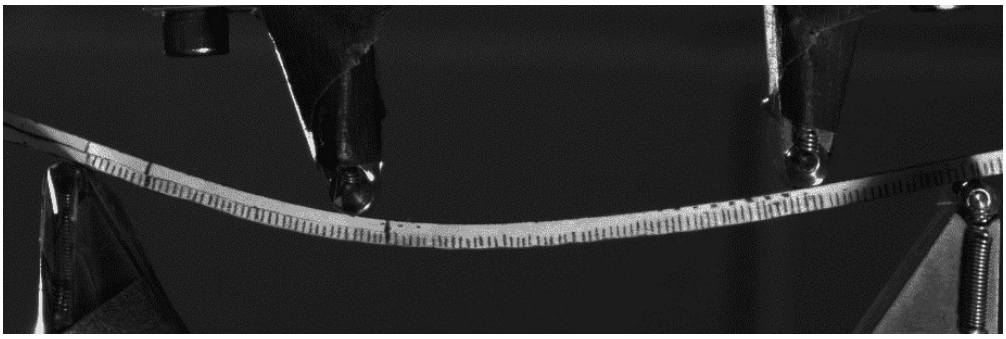

Figure 3.15: UD specimen at high deflection during 4ENF test showing asymmetry

not necessarily the case.

3.3.3.2 Experiment

While the 4ENF test is the simplest of the proposed tests for steady-state, mode II crack-growth, it still comes with issues to be overcome. Without additional measures, the specimen will begin to slide [29]. The phenomenon is not documented in all cases, so it appears to be relative to the specimen being tested. The specimen is likely to slide in the fixture at relatively high deformation, so thinner specimens with a lower flexural modulus and higher fracture toughness are more likely to slide. This is due to the asymmetry of which an ENF specimen will deform when loaded, causing the end with the pre-crack to have a higher angle of contact with the roller relative to the original position. At high deformations, this end will become closer to parallel with the loading as opposed to perpendicular. Figures 3.15 and 3.16 shows this issue for the tests conducted.

Literature has shown different ways to combat this issue of sliding. Wang et. al. used rubber bands to hold the specimen in place at the support rollers [24], Schuecker and Davidson used a fixture on the pre-cracked end of the specimen to hold it and keep it from sliding [29], and Kageyama et. al. used a PTFE film between the rollers and the specimens to reduce friction, and in turn, reduce the stick slip seen in the load-displacement curve [30].

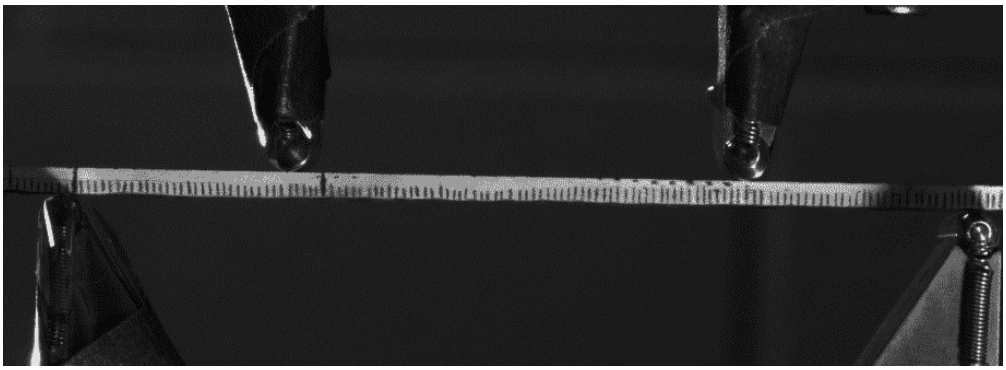

(a) Beginning of test

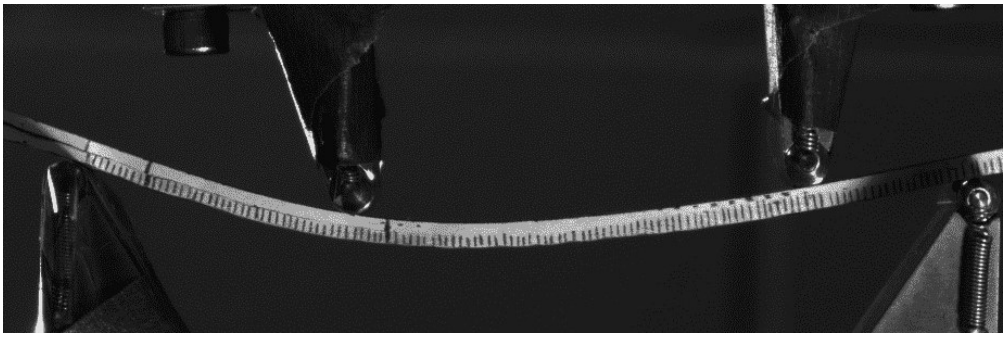

(b) End of test

Figure 3.16: Images showing relative sliding of specimen on fixture.

The method by Wang was trialed first to combat the sliding of the specimen. The reason that this was chosen first is because it would not completely constrain the specimen from sliding, and it would put fewer artificial loads into the specimen. As opposed to constraining the pre-cracked end, the rubber bans did not add any lateral load into the specimen, and it required less post-processing of the specimen. This method was found to eliminate the relative sliding in some specimens, but there was still reduced sliding in others. Due to the inconsistencies in the specimens and the relative sliding that still existed in some, another method was pursued.

The next method investigated was to reduce the friction in the two loading rollers and the support roller under the pre-crack. Kageyama et. al. found this to reduce the stick-slip in the load-deflection curve, and this is what the relative sliding appears as in the data. The friction was reduced by using a 0.001 in thick polyimide film between the rollers and the specimen. When this is implemented, there is still some sliding, but this can be expected in a four-point bend test. Instead of the stick-slip condition seen before, the sliding was gradual throughout the test, and it was reduced when compared to the original tests.

The stick-slip condition was nearly, if not completely, eliminated by reducing the friction in the loading rollers and support roller under the pre-crack. There is still some relative sliding between the specimen and the fixture, and this was sought to be eliminated by increasing the friction at the fourth roller. This would allow for the beam to be nearly completely simply supported with no sliding allowed on the end of the specimen without the pre-crack and reduced friction sliding at the end with the pre-crack. The increase friction is achieved by using a thin piece of high-grit sandpaper between the roller and the specimen with the grit side facing the specimen. When this was implored along with the polyimide film between the loading rollers and the support roller under the pre-crack, no stick-slip or

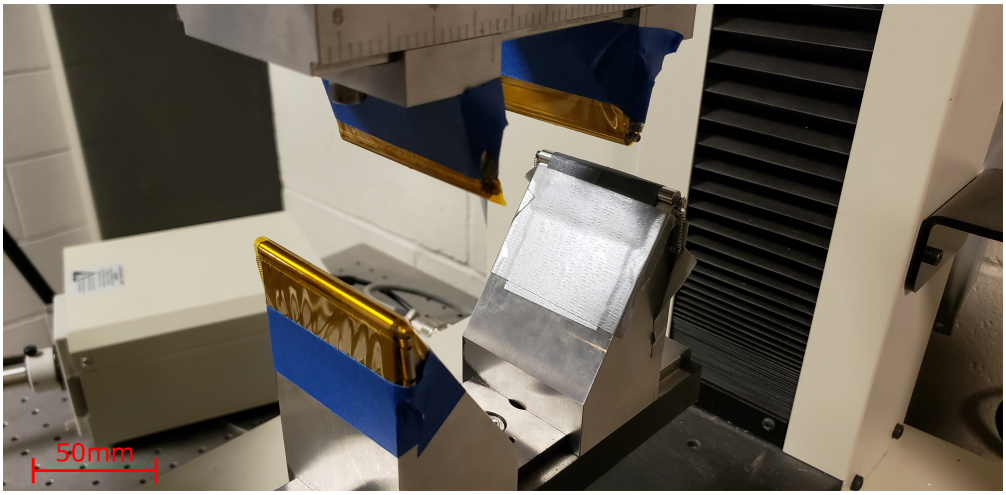

Figure 3.17: 4ENF fixture with orange polyimide film to reduce friction and gray sandpaper to increase it

Table 3.7: 4ENF Sample Dimensions [mm]

Specimen	**b**	**h**
UD1	25.7	1.805
UD2	25.6	1.809
UD3	26.2	1.820
UD4	25.4	1.789
Q3D1	25.3	1.796
Q3D2	25.2	1.863
Q3D3	25.7	1.877
Q3D4	25.7	1.866

relative sliding is seen. The final setup of the fixture is seen in figure 3.17. Figure 3.18 shows how this fixture's adaptation changes how the specimen is sliding on the fixture.

For the 4ENF tests conducted in this study, the spans are changed from the previous ENF tests and what is seen in literature [5, 30, 31]. The geometry of the test is show in table 3.7.

A d/2L value of 0.5 is used to remain consistent with literature [5, 30, 32, 33, 34], and this is the determining factor for the geometry of this test. The loading span is set to 63.5mm to ensure that two full interlaminar tows beyond the initial crack tip are within the loading span. With the standard d = 50mm, the second tow is at/beyond the second loading roller,

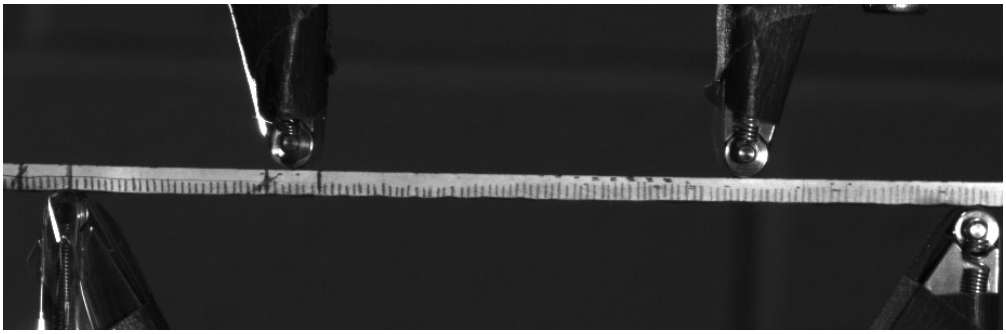

(a) Beginning of test

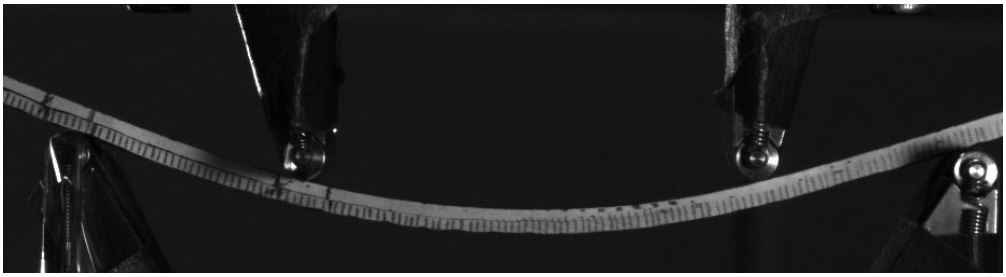

(b) End of test

Figure 3.18: Images showing no relative sliding of specimen on fixture.

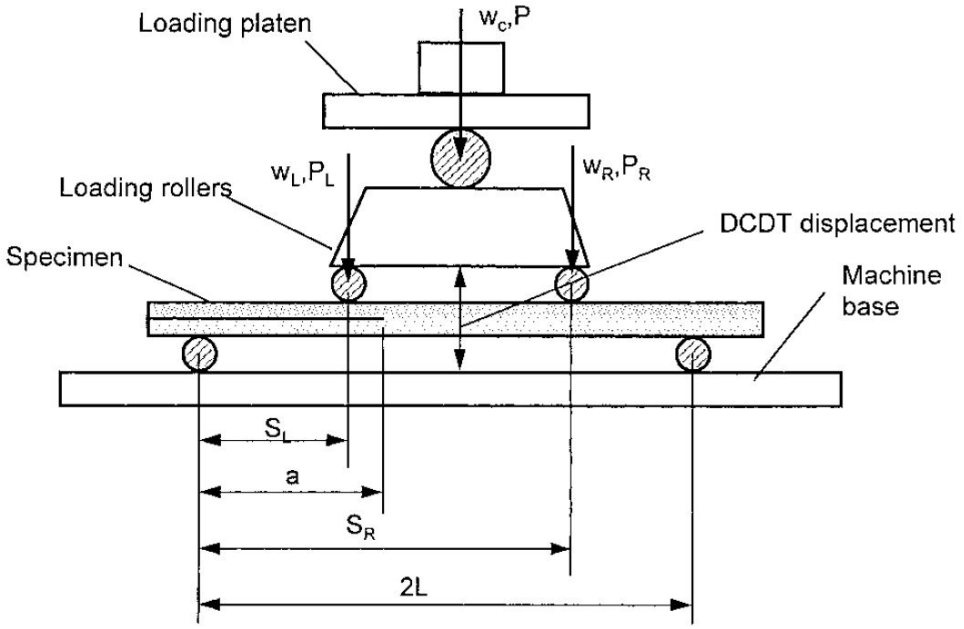

Figure 3.19: Representation of nomenclature for 4ENF test [5]. Not shown is d, which is the spacing between the loading rollers.

Table 3.8: 4ENF Parameter Dimensions [mm]

Parameter	**Value**
a	35
L	63.5
S_L	31.75
S_R	95.25

Figure 3.20: 4ENF setup showing cameras of both sides of the specimen

and the influence of the roller is not discernible from the influence of the interlaminar two. For this reason, the inner span is increased, the the outer is also increased to maintain the d/2L ration of 0.5. These testing parameters are summarized in table 3.8

Due to the $[0°/60°/\text{-}60°]_S$ not having the 0°ply at the interface and the interlaminar tows of the Q3D not always being located in the center of the beam, two cameras are used to record the crack growth. Figure 3.20 shows the cameras on both sides of the specimen. The sides of the specimen are painted white, and marks are made every millimeter such that an accurate measure of the crack length can be taken. The cameras are each taking images at 1 $\frac{\text{image}}{\text{second}}$ to match the data recording of the testing frame at 1 Hz. The tests are also conducted at 0.5 $\frac{\text{mm}}{\text{min}}$ to coincide with the standard for ENF and the paper proposing 4ENF to measure mode II fracture toughness [5]. An initial crack length, a_o, of 35 mm to put the crack tip just inside the first loading roller.

Table 3.9: 4ENF Mode II Averages $\left[\frac{\text{J}}{\text{m}^2}\right]$

	UD	**Q3D**
Initial	759.5	697.3
Steady-State	449.4	653.1

3.3.3.3 Results

In the 4ENF tests, there is no need to perform PC and NPC tests. This is because there is continuous crack propagation throughout the 4ENF test, so only the initial crack propagation is considered NPC, and the rest is considered PC. For this study, the initial crack propagation is ignored because the steady-state crack resistance is desired. As seen in the mode I and mode II tests, the Q3D architecture shows its advantage beyond initial crack propagation, and this is where the comparison will be drawn.

The values for fracture toughness through the 4ENF test are found in a similar manner to the ENF test. Similar to the ENF test, the compliance calibration is also used, and these measurements are taken at crack length of 25mm and 45mm to keep with the ±10mm from the ENF test. The main difference, however, comes from the equation used to calculate the fracture toughness. For ENF, the G_{II} value is dependent upon the crack length, but with 4ENF, it is not. Beam theory shows this relationship, but in reality, the loading rollers have an effect on the G value [5]. The equation used to calculate G_{II} for the 4ENF test is:

$$G_{\text{II}} = \frac{P^2 m}{2b} \tag{3.5}$$

Table 3.9 shows the average values obtained in the initial and steady-state crack growth regimes of the R-curves. In the steady state regime, these values are about 20% smaller than what is obtained through ENF. This is contradictory to what is observed by Martin [5]. However, Martin mentioned that the specimens were tested a year later, and moisture

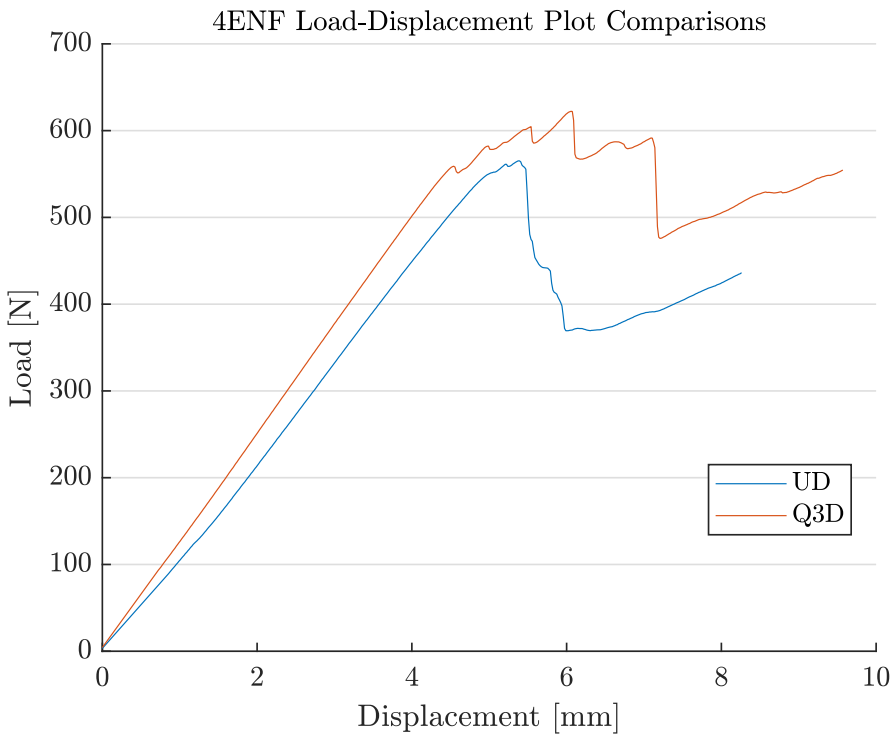

Figure 3.21: Comparison of representative load-deflection curves from UD and Q3D 4ENF tests

absorption could cause an increase in the perceived toughness of the composite. A different span is used in the ENF and 4ENF tests in this study, and that could have an effect as well.

Figure 3.21 shows a comparison of representative curves from the UD and Q3D 4ENF specimens. This shows that the Q3D maintains a higher peak load, and it does not have that immediate drop. This would require more energy to achieve the same deflection and damage in the Q3D specimen as is seen in the UD specimen. This observation also agrees with the work done comparing Q3D and UD in out-of-plane impact tests. Liu, Rosario, Klann, and Zhou found that a Q3D structure has lower energy absorption and lower deflection than a UD sample, but it also has a much smaller damage area, leading to a higher specific energy absorption [2, 19, 20]. Coppens and Liu also found that a larger amount of energy is required to fully perforate a Q3D laminate compared to a UD laminate [35]. The higher fracture toughness for steady-state crack growth along with the higher load sustainability

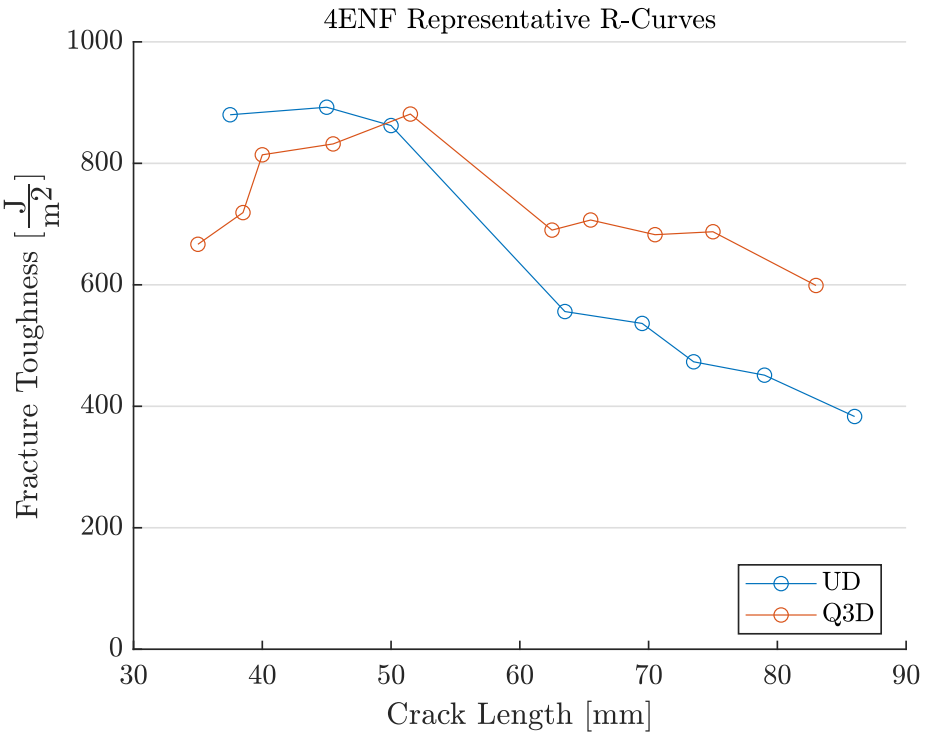

Figure 3.22: Comparison of representative R-Curves from UD and Q3D specimens

point towards this higher specific energy absorption and larger required energy for perforation found in literature.

A similar trend to the mode I R-curves is shown for the mode II R-curves in figure 3.22. Initially near the pre-crack, the Q3D has a fracture toughness which is lower than that of the UD. However, beyond 50mm, the effect of the through thickness tows is shown with a higher fracture toughness. Both the UD and the Q3D show the same downward trend beyond the large crack growth from ∼50-∼65mm. This shows that crack propagation is similar for both the UD and the Q3D between the interlaminar tows, but the interlaminar tows have a significant improvement on the fracture toughness: nearly 45%. More R-curves for both architectures are shown in the appendix.

In the mode I specimens, the higher fracture toughness comes from the interlaminar tows physically bridging the gap and breaking at a higher load. However, this is not the

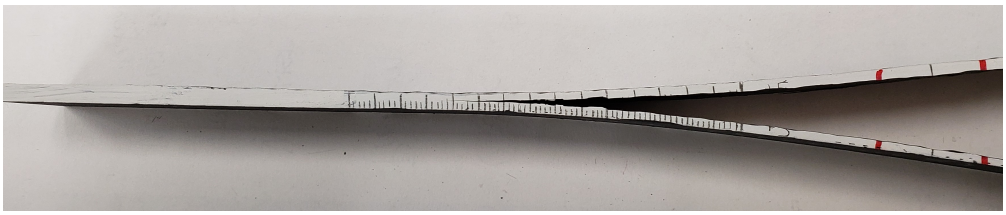

(a) UD specimen after 4ENF

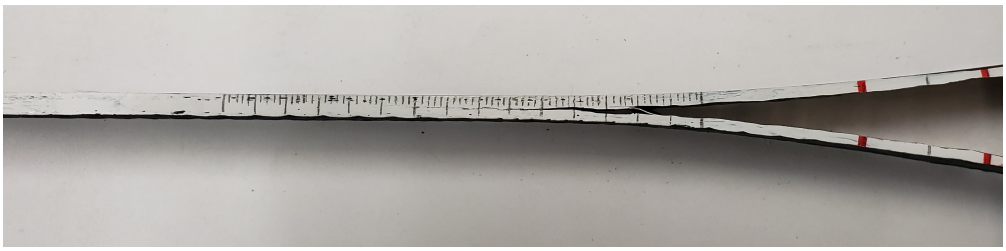

(b) Q3D specimen after 4ENF

Figure 3.23: Images showing relative sliding of specimen on fixture.

case for mode II. In mode II tests, the interlaminar tow of the Q3D laminate does not break. This is seen post-mortem in figure 3.23. In these images, the same crack separation is given at the location of the support during the 4ENF test. The UD specimen shows less resistance to being pulled apart along the length of the crack where the Q3D is being held together by that interlaminar tow. This would mean that for the same crack growth, the Q3D structure will likely have better in-plane properties. This carries significant meaning for this study because this architecture is being investigated for a crash-sensitive component in an automotive vehicle.

Chapter 4: In-Plane Characteristics

4.1 Background

The in-plane properties of the Q3D architecture are also investigated in this study. The main purpose is to gather data for material characterization such that a material model can be made. This material model would be applied to the hat section that this material is being investigated for, and the theoretical results can be compared with the experimental results.

The in-plane results can also be compared experimentally with UD and 2DW architectures if the same fibers are used. This would show the true effect of the 3 dimensional braiding on the in-plane properties of the laminate as compared to a UD or traditionally woven laminate.

4.2 Tension

4.2.1 Experiment

The tensile tests for the Q3D material are performed in accordance with ASTM D3039 [36]. Specimens are tested at a rate of 2 $\frac{\text{mm}}{\text{min}}$ on a MTS 810 hydraulic test frame. A typical gage length of 33.5 mm is used, and strain measurements are made by utilizing a laser extensometer to measure strain before failure. After failure, the reflective tape on the specimen often falls off or moves, thus making the strain reading inaccurate. The experimental setup is shown in figure 4.1 and the specimen with the reflective tape is shown in figure 4.2. The tabs are made from a woven fiberglass composite and adhered by using 24 hour, room-temp cure epoxy. The tabs are 8.89 mm thick such that the MTS machine could be used for its high load capacity. The dimensions for the specimens are shown in table 4.1. In this table,

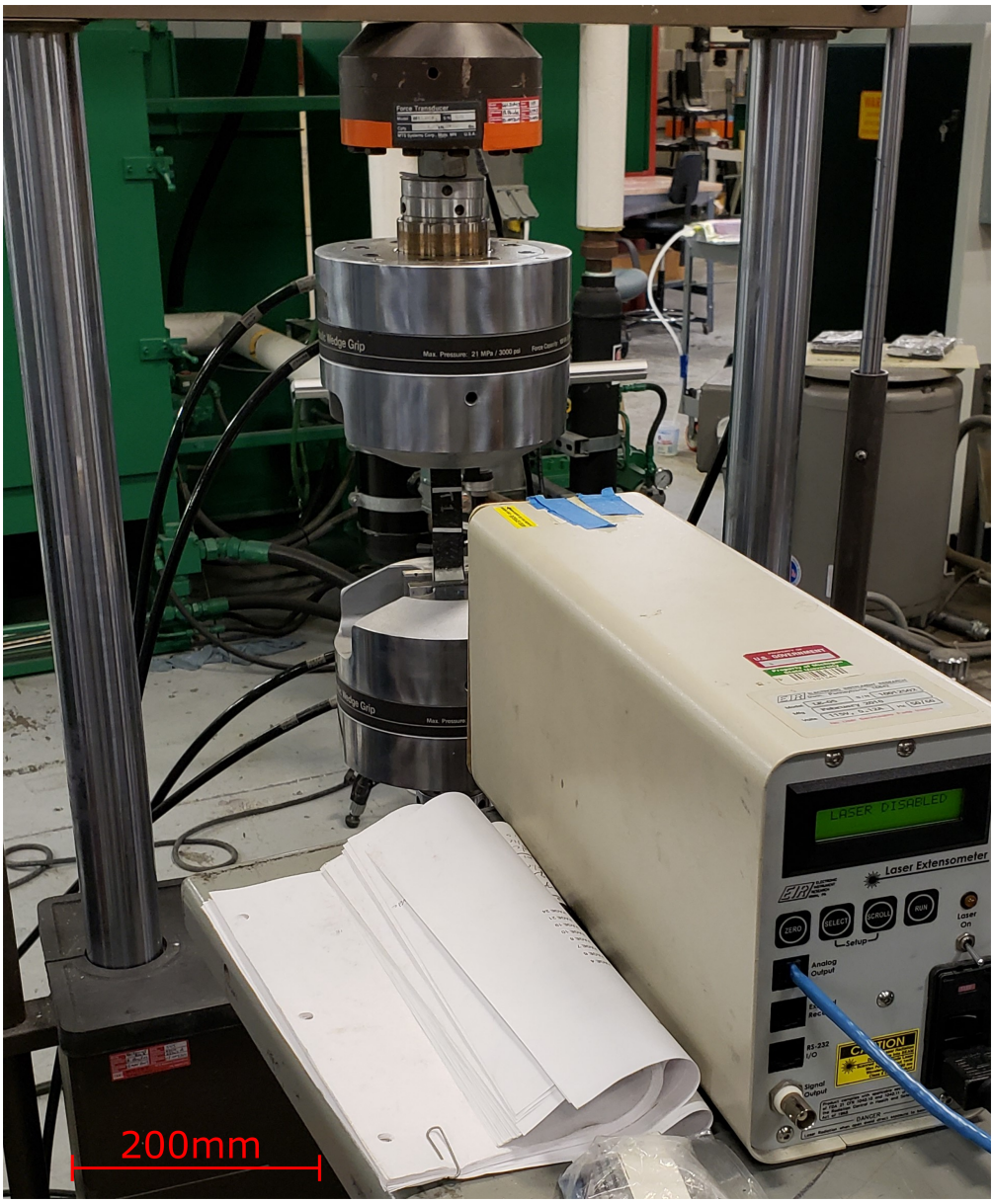

Figure 4.1: Setup of tensile tests showing laser extensometer and specimen

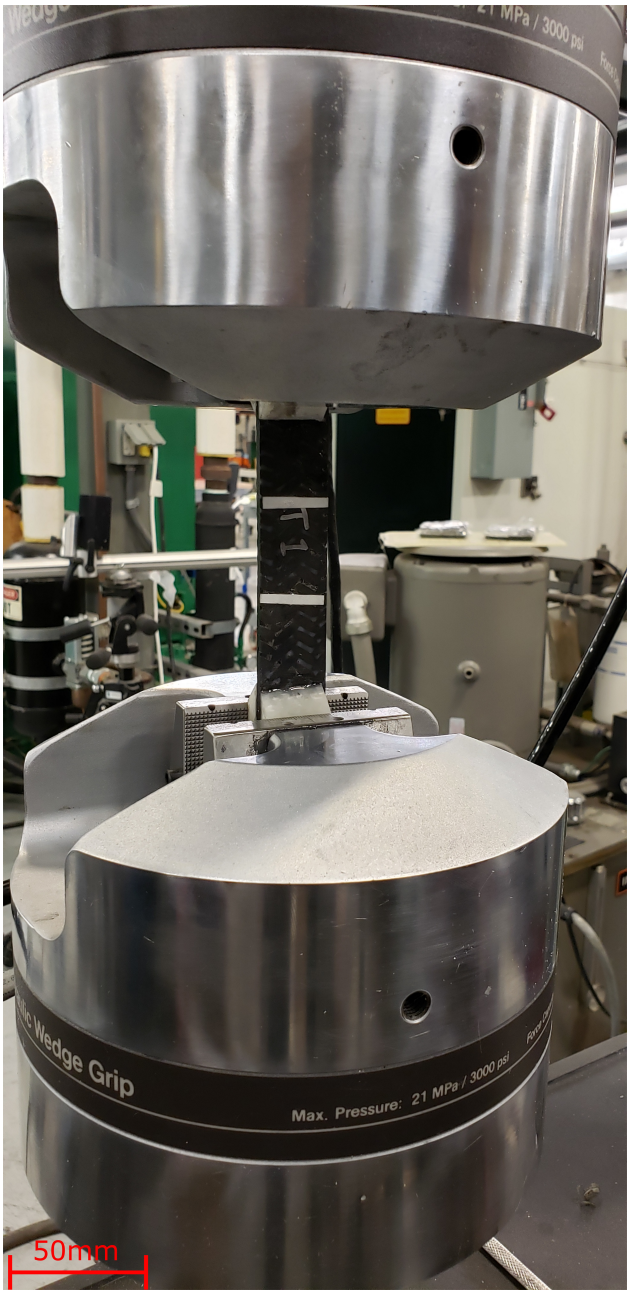

Figure 4.2: Close-up of specimen showing the silver tape that is reflecting the laser

Table 4.1: Tensile Sample Dimensions [mm]

Specimen	**b**	**h**	**L_g**
Q3D1	26.1	4.380	103.2
Q3D2	25.1	4.813	94.6
Q3D3	25.5	4.353	101.7

L_g refers to the length between the reflective tape used by the laser extensometer to measure the strain. The overall length of 250mm and general width of 25.4mm is recommended by ASTM D3039 [36].

4.2.2 Results

The stress and strain for the test are calculated using equations 4.1 and 4.2, respectively.

$$\sigma = \frac{P}{A} \tag{4.1}$$

$$\epsilon = \frac{\delta}{L_g} \tag{4.2}$$

After failure, the laser extensometer can no longer accurately measure the strain, so to obtain a full stress-strain curve to include after failure characteristics, a relation with the machine displacement output is made. A correction value is obtained by doing a linear regression between the displacement given by the laser extensometer and by the test machine. This correction factor is then applied for all of the machine displacement values to obtain strain beyond initial failure. These stress-strain curves are shown in figure 4.3. The values for the ultimate stress and elastic modulus are then shown in table 4.2.

Figure 4.4 shows the failure of each of the specimens. Each failure is slightly different with Q3D1 and Q3D2 failing at the top of the specimen as opposed to in the middle like

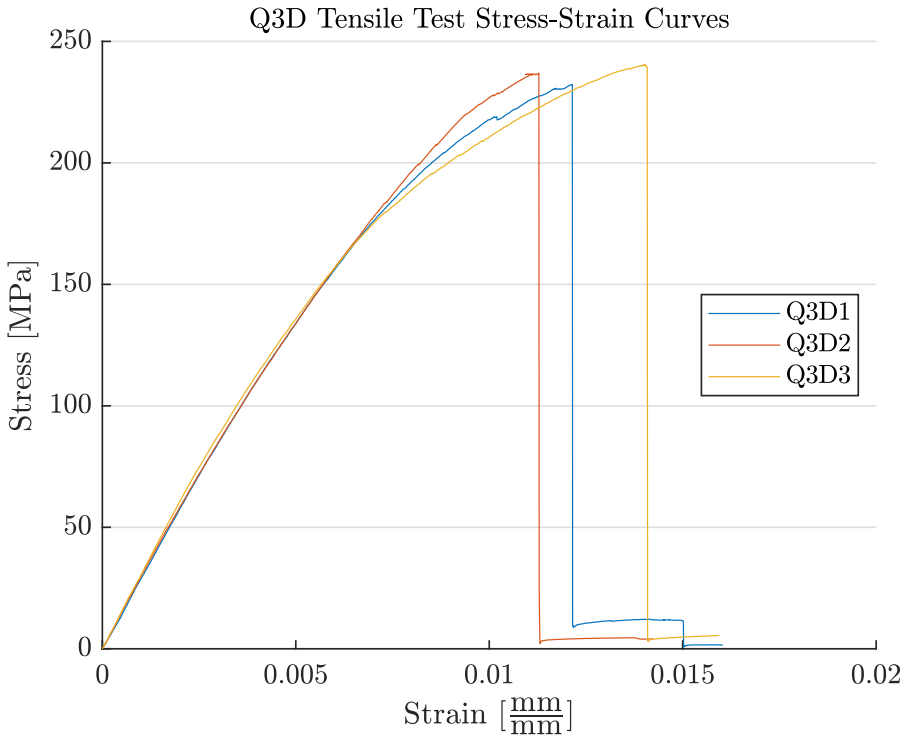

Figure 4.3: Stress-strain curves from Q3D tensile tests

Table 4.2: Q3D Tensile Properties

Specimen	**Ultimate Stress [MPa]**	**Elastic Modulus [GPa]**
Q3D1	232.3	27.28
Q3D2	236.9	27.38
Q3D3	240.4	28.39
Average	236.5	27.68

Figure 4.4: Tensile failures of the Q3D1, Q3D2, and Q3D3 specimens, respectively

Q3D3. The Q3D2 fails across the specimen where the Q3D1 and Q3D3 fail in the direction of the -60°tow. This is more evident in the Q3D1 specimen with failure occurring completely parallel to the -60°tow.

4.3 Flexural

4.3.1 Experiment

The flexural properties of the Q3D composite are determined by following ASTM D7264 [37]. Instead of using the standard width of 12.7 mm, a width of 40mm is used. This is because the standard prescribes a width of two unit cells for textile composites. The standard span-to-thickness ratio of 32:1 is maintained. The typical thickness of a specimen is 4mm, and thus the support span, L, used is 128mm. Figure 4.5 shows the nomenclature for the test,

Table 4.3: Flex Test Dimensions [mm]

Specimen	b	h
Q3D1	39.45	4.233
Q3D2	40.29	3.889
Q3D3	39.50	4.250
Q3D4	38.85	4.118
Q3D5	38.90	4.127

and table 4.3 shows the specimen dimensions. For the flex tests, h is the full thickness and not the half thickness. Figures 4.6 and 4.7 show the specimen mid-test. The tests are conducted with a crosshead displacement rate of $1\frac{\text{mm}}{\text{min}}$.

4.3.2 Results

Equations 4.3 and 4.4 are used to calculate the stress and strain of the specimen in the flexural test. The load is taken from the load cell in line with the loading roller, and the displacement is taken from the crosshead displacement of the machine. This is used because the output was confirmed to be within 0.5% by a laser extensometer for all expected loads.

$$\sigma = \frac{3PL}{2bh^2} \tag{4.3}$$

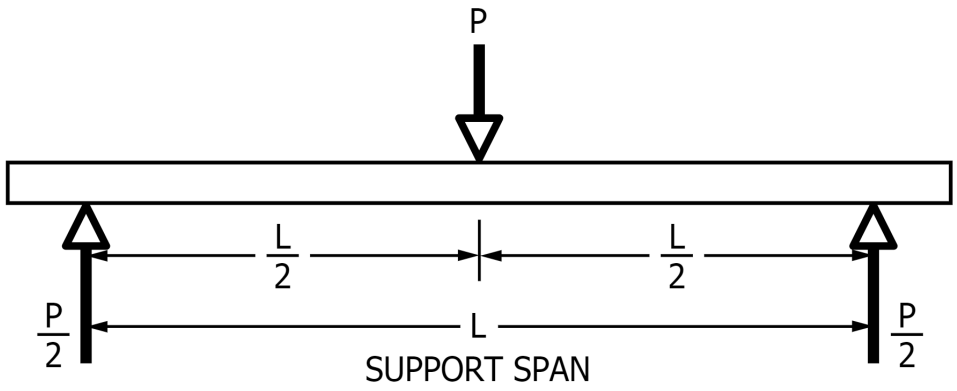

Figure 4.5: Diagram showing flexural test nomenclature

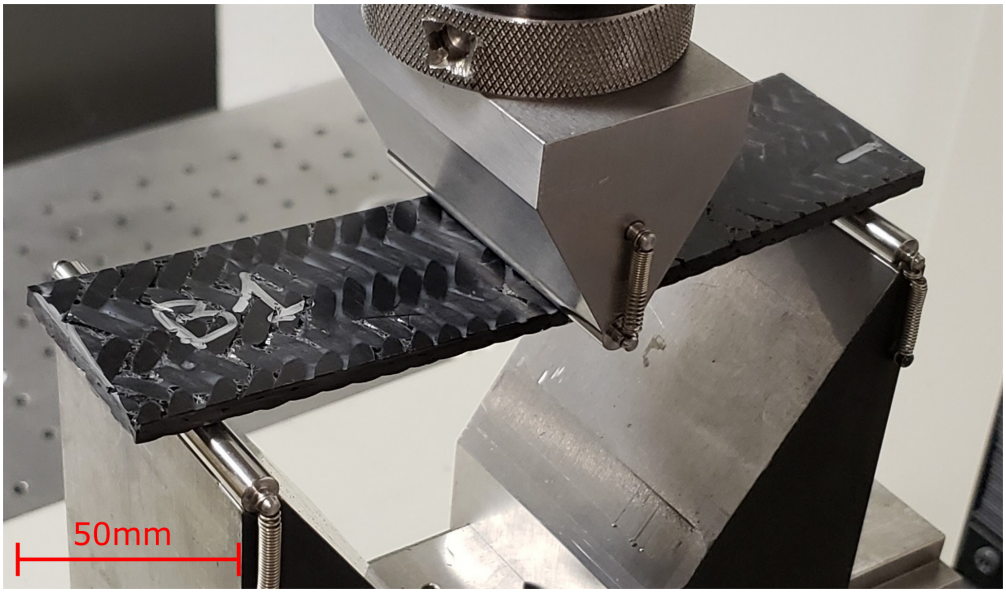

Figure 4.6: Isometric view of 3 point bend setup

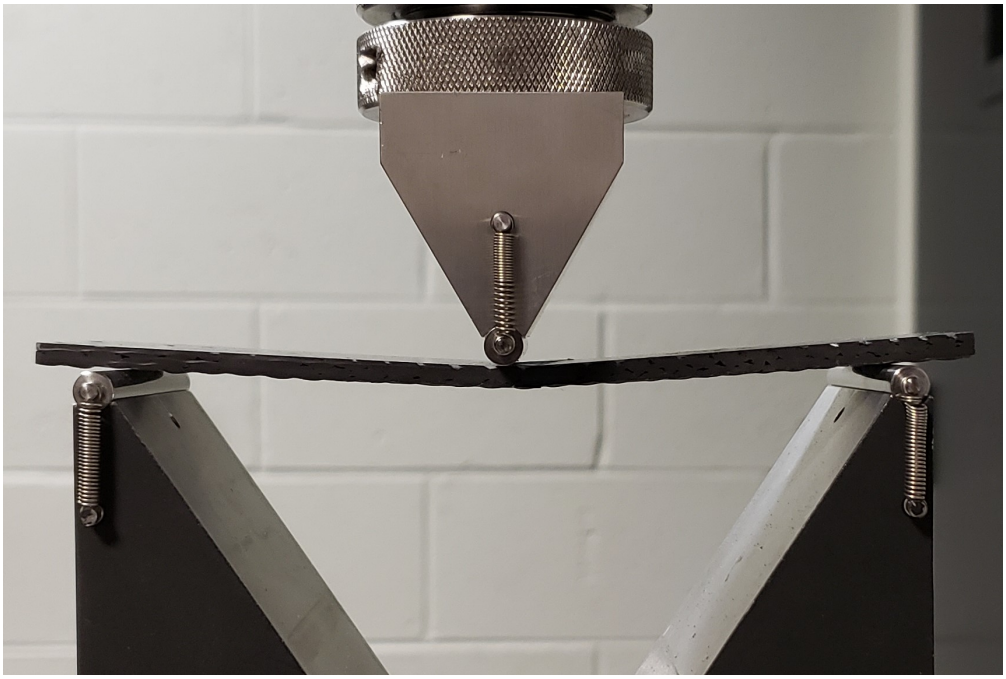

Figure 4.7: Front view of 3 point bend specimen mid-test

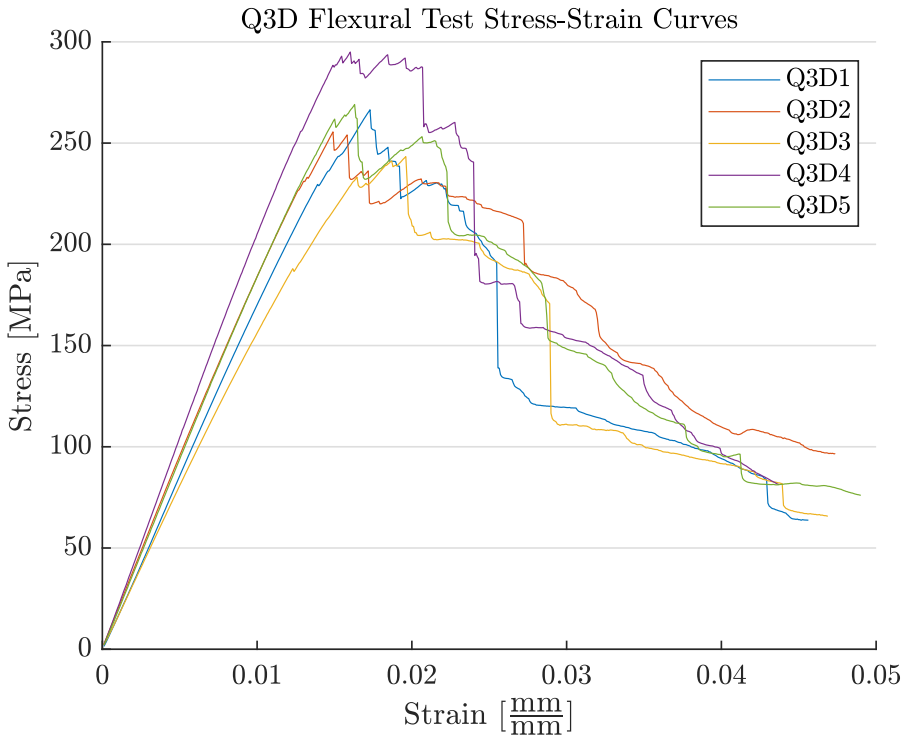

Figure 4.8: Stress-strain curves from Q3D flexural tests

$$\epsilon = \frac{6\delta h}{L^2} \tag{4.4}$$

From the results of the flexural tests, the average ultimate stress is found to be 265.9 MPa with a flexural modulus of 18.49 GPa. Figure 4.8 shows the stress-strain curves from the test. Strain values are taken from 0.001 to 0.003 $\frac{\text{mm}}{\text{mm}}$.

Initial failure occurs on the compression side of the specimen. Figures 4.9 and 4.10 shows failures for the Q3D4 specimen. The compression failure occurs first at a stress of just under 300 MPa and a strain of 0.015 $\frac{\text{mm}}{\text{mm}}$. Failure occurs solely on the compression side of the specimen until a strain of about 0.0375 $\frac{\text{mm}}{\text{mm}}$ where the first failure is seen on the tensile surface of the specimen. Table 4.4 shows the properties for each specimen tested along with the average for the five.

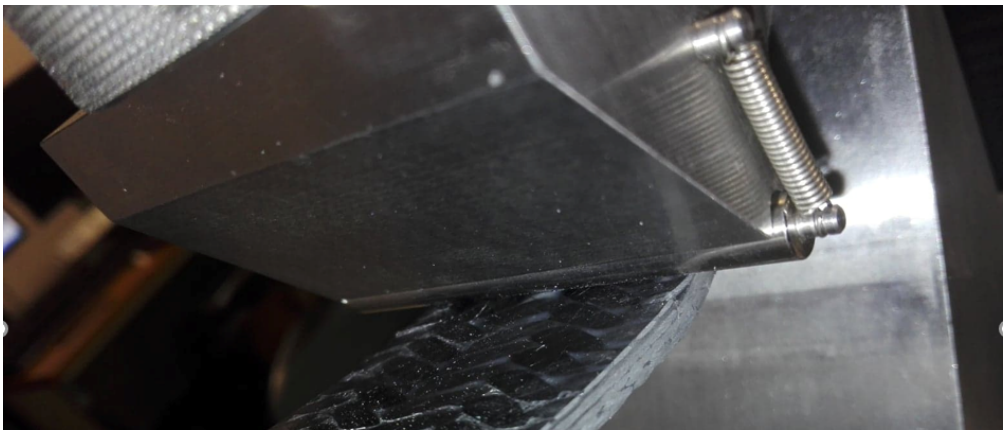

Figure 4.9: First failure at the compression side of the Q3D4 specimen at the peak load

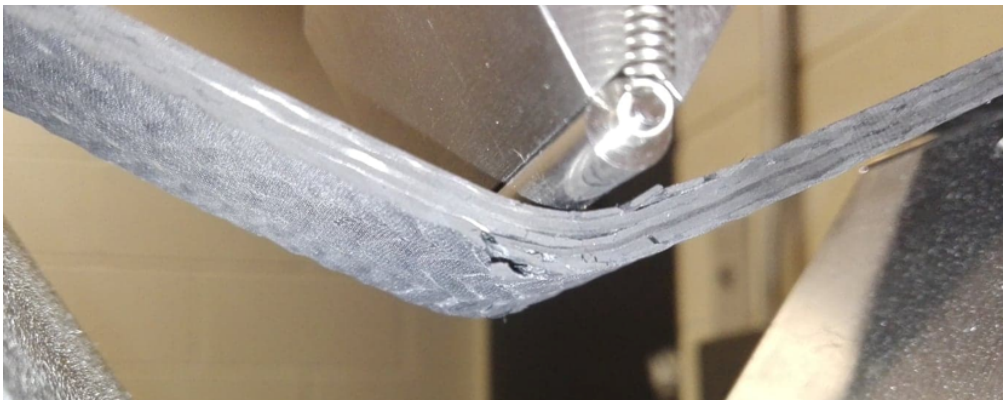

Figure 4.10: Failure at the tensile side of the Q3D4 specimen

Table 4.4: Q3D Flexural Properties

Specimen	**Ultimate Stress [MPa]**	**Flexural Modulus [GPa]**
Q3D1	266.5	17.14
Q3D2	255.6	19.17
Q3D3	243.3	16.31
Q3D4	295.0	20.93
Q3D5	269.1	18.93
Average	265.9	18.49

Chapter 5: Hat Section

The purpose of this work is to test the feasibility of using a CFRP composite as the material for the roof-header in an automotive vehicle. The critical section of this roof-header is deemed the "hat section," and figure 5.1 shows a cross section of the studied hat section with dimensions removed. Bayraktar used a 3D woven composite in a similar hat section and found that the 3D woven composite will absorb less energy than a comparable steel hat section, but it will be more efficient in terms of energy absorption per mass [21]. When compared to the optimized hat section, the composite beam did not perform as well, but the composite beam was not optimized at all.

Figure 5.1: General cross section of the hat section

5.1 Manufacture

A special tool is required to create the hat section, and it is machined out of aluminum. The tool is aluminum so that it is durable and sand-able for multiple infusions. The aluminum will also be able to handle the heat of the cure and is light enough to be transferred from the work area to the oven by one person. It is also manufactured such that the resin inlet and the vent are integrated into the tool. The tool is tapped with 1/4" NPT threads such that barbed tube fittings can be placed on either end. An image of the tool is shown in figure 5.2.

Infusion of the hat section is very similar to that of a flat plate. The major difference between the two is that the hat section needs pleats in the concave sections of the mold to reduce bridging in the bag.If the bag bridges, there is no pressure in the concave section, and the preform with not take the shape of the tool. This also gives an area where resin will pool and is a likely site for voids. The pleats used for this part are shown in figure 5.3.

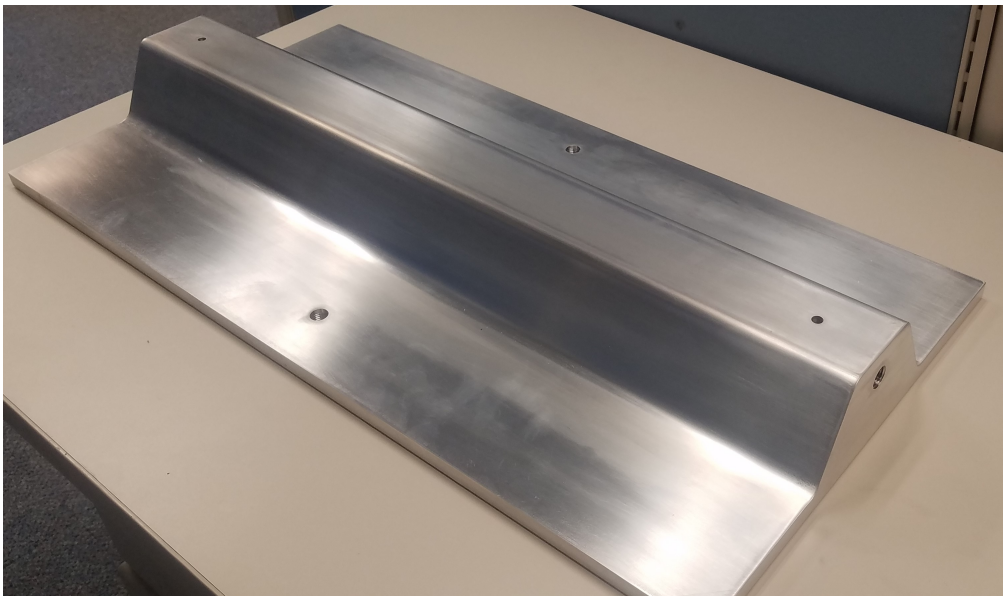

Figure 5.2: Tool used to manufacture hat section

When vacuum is first pulled, the pressure is only brought to ∼20inHg. This is so that there is partial vacuum holding the bag in place, but it can still be easily manipulated. The crease that is caused by the pleats is then manipulated to be on top of the concave section. When full vacuum is pulled, instead of the bag bridging, the bag will come into full contact with the preform because of the extra bagging from the crease. Once this has been done and all bridging has been eliminated, that infusion process can continue as normal. Figure 5.4 shows a hat section during the infusion process.

The Q3D material also comes with issues when it comes to manufacturing. Because it is a single preform and not multiple layers, this can cause poor drapability. There were issues involving draping the Q3D preform onto the hat section mold which caused bridging in the concave section. The effect of this bridging can be seen in figure 5.5 where there is an excess of resin in one part of the component. It is possible to overcome this, but greater care needs to be taken in manufacturing. The bridging can also be overcome with more gradual corners.

A flat plate of the same material is also made, and it is bonded to the bottom of the hat section. It is crucial that this flat plate is made of the same or similar material because if it has a different stiffness, this could cause premature or uncharacteristic failure in the hat section. This flat plate is bonded to the bottom of the hat section such that the beam bends along its span as opposed to opening up and becoming wider. Along with the Q3D material, hat sections and flat plates made from A&P Technologies triaxially braided [0°/60°/-60°] carbon fiber are also manufactured for a comparison to a textile composite. Previous tests done by Ford show delamination in the center at the hat section that the Q3D seeks to solve. Figures 5.6 - 5.8 shows example hat sections that will be tested.

(a) Pleat in the sealant tape

(b) Pleat in the vacuum bag

Figure 5.3: Pleats in the vacuum bag of a hat section infusion

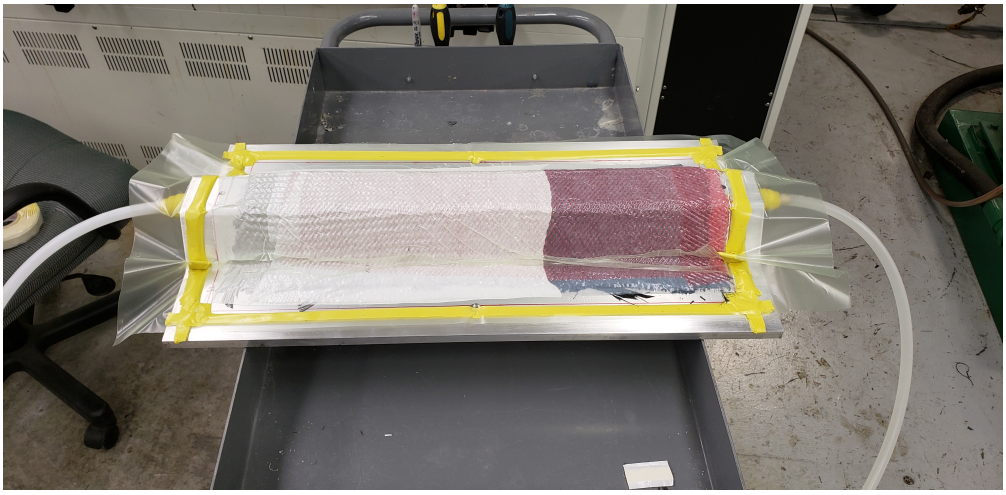

Figure 5.4: Infusion of a hat section

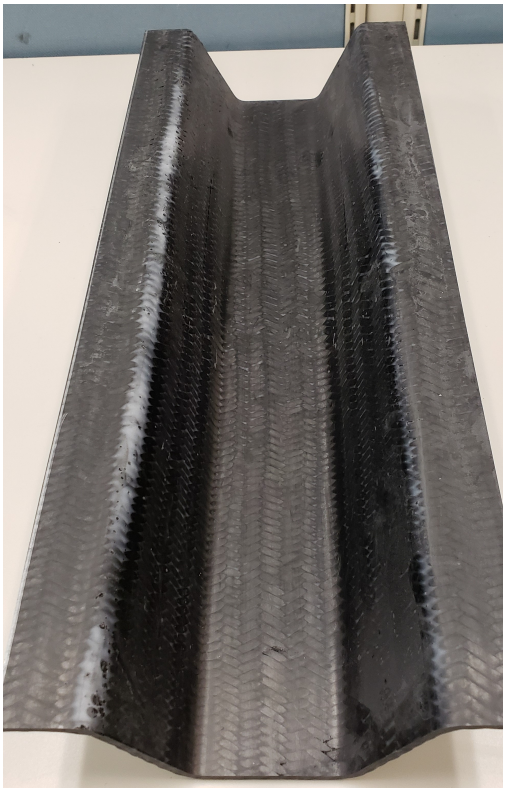

Figure 5.5: The resin rich area on the left side of the part is a direct effect of preform bridging during composite manufacture

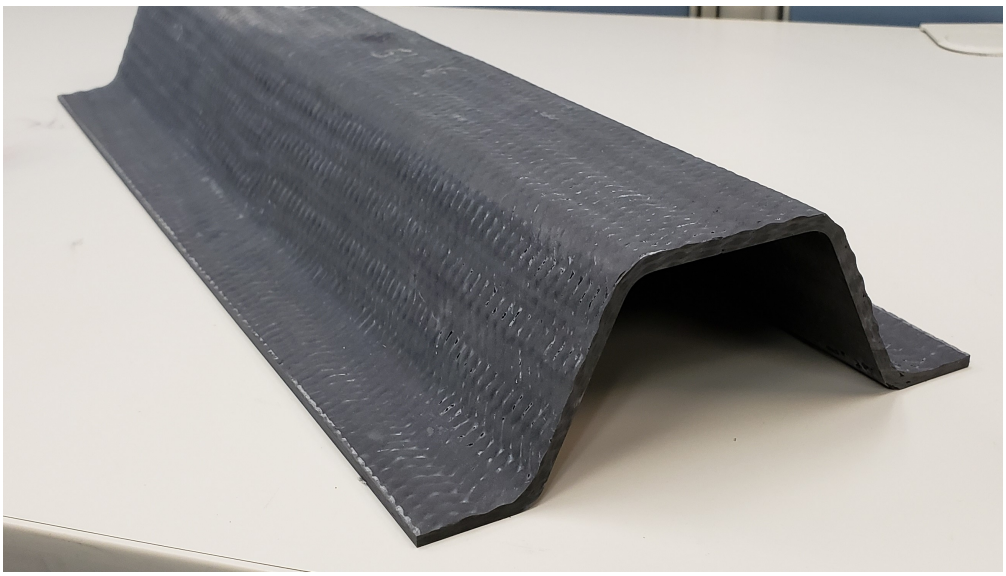

Figure 5.6: Isometric view of a Q3D hat section

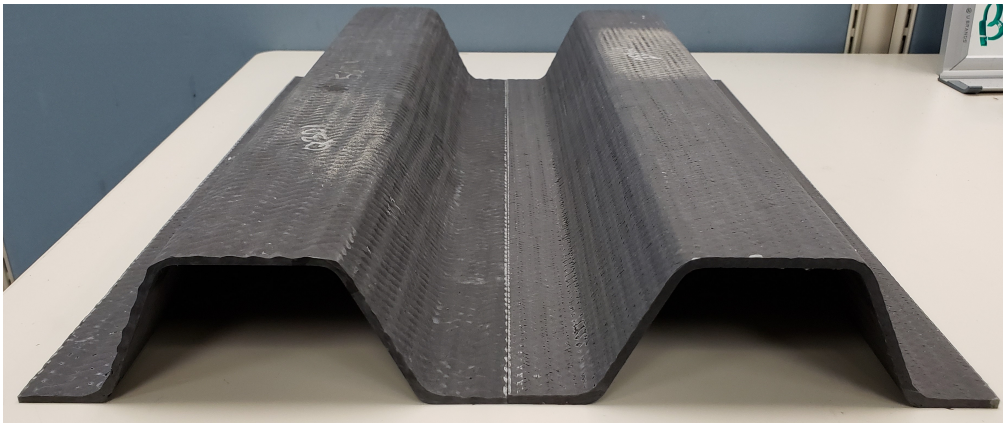

Figure 5.7: Comparison of Q3D and 2DW hat sections

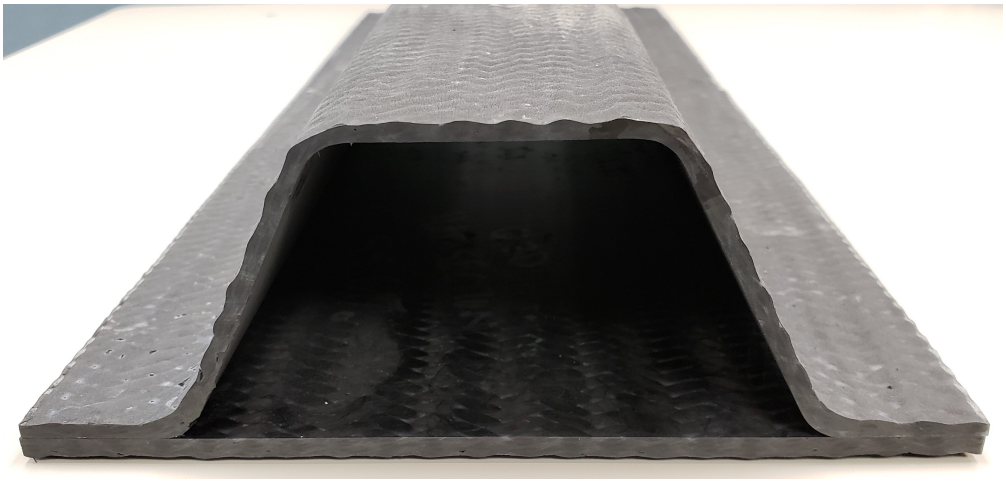

Figure 5.8: Q3D hat section with flat plate to be bonded for testing

5.2 Experiment

The hat section has not been tested as of the writing of this thesis, but tests are currently in progress. The test being performed is a dynamic 3 point bend test to simulate an impact occurring transverse to the length of the hat section. Both the textile hat section and the Q3D hat section will be tested, and they will have similar thicknesses to draw conclusions based simply upon the fiber architecture. 3 specimens of each are tested to show repeatability of the tests such that an accurate conclusion can be drawn about the feasibility of using the Q3D architecture for structural applications.

Chapter 6: Conclusion

6.1 Summary and Conclusions

Braiding a composite structure with the bias tows spanning multiple layers has shown to improve the interlaminar fracture toughness of laminated composite materials. Under mode I loading, a fracture toughness increase of over 20% is found when compared with UD and a traditionally braided laminate of the same fiber orientation. It has also been found that the Q3D composite requires more energy for the same amount of crack propagation compared to the UD and 2DW in both mode I and mode II testing. Using the energy absorption is found to be a good method to compare the fracture performance of composites because there is no discrimination due to the number of times that the crack propagates during the test. The Q3D architecture also shows an even greater increase in mode II fracture toughness with 47.3% and 18.4% increase over UD and 2DW composites, respectively when looking at the PC condition for the 3 point ENF test.

The 4ENF test was also investigated to determine its effectiveness for producing an R-curve for mode II tests. There are initial issues with the tests due to specimen sliding, but by reducing the friction of the loading rollers and support roller under the pre-crack and increasing the friction of the support roller under solves this issue. An R-curve can be generate for mode II fracture toughness because the 4ENF test will give stable crack growth. When comparing the fracture toughness values of the 4ENF test to the ENF tests, the initial fracture toughness is over predicted, but the steady-state fracture toughness is under predicted.

At initial crack growth, the Q3D architecture does not perform as well as the UD, but

this agrees with the mode I results and the mode II results from ENF. However, in the steady regime of crack growth, Q3D shows an average 41.3% increase in fracture toughness when compared to a UD laminate with the same fiber orientation. This increase is also maintained as the crack propagates.

Tensile and flexural tests have been conducted on the Q3D composite to view the stress-strain behavior. The results from these tests will also be compared to a UD laminate to compare properties and investigate if this fiber architecture causes any degradation in the in-plane properties.

The tri-axial, Q3D preform used in this study is braided into a tube, but when it is cut lengthwise and spread, it is able to be draped over a tool with curvature to make a complex part.

6.2 Future Work

Beyond the work presented in this paper, a better comparison of the Q3D architecture with that of UD and 2DW should be determined for in-plane properties. This will give a better understanding of how the out-of-plane braiding degrades the in-plane properties of the composite. The Q3D architecture will also be tested in the hat section structure to determine is the fracture toughness benefits seen in the mode I and mode II testing translate well when applied to a structure.

Along with the tensile and flexural in-plane results that have been obtained, compressive tests will be conducted for the material model and for a comparison to a UD laminate. The experimental results for in-plane properties and fracture toughness will also be used to create a material model for the Q3D architecture. Once this material model is made and confirmed for the in-plane and fracture toughness experiments, the hat section will be

simulated with the material model to determine how well the simulation model predicts the actual performance and failure of the structure. abc

APPENDIX

Figure A.1: UD mode I R-curves

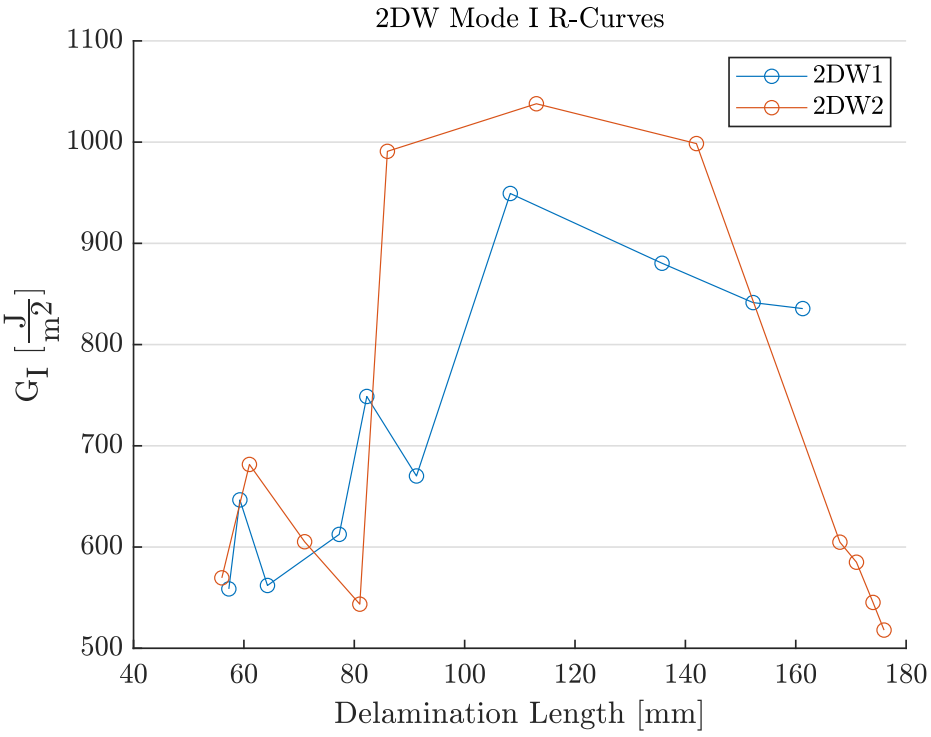

Figure A.2: 2DW mode I R-curves

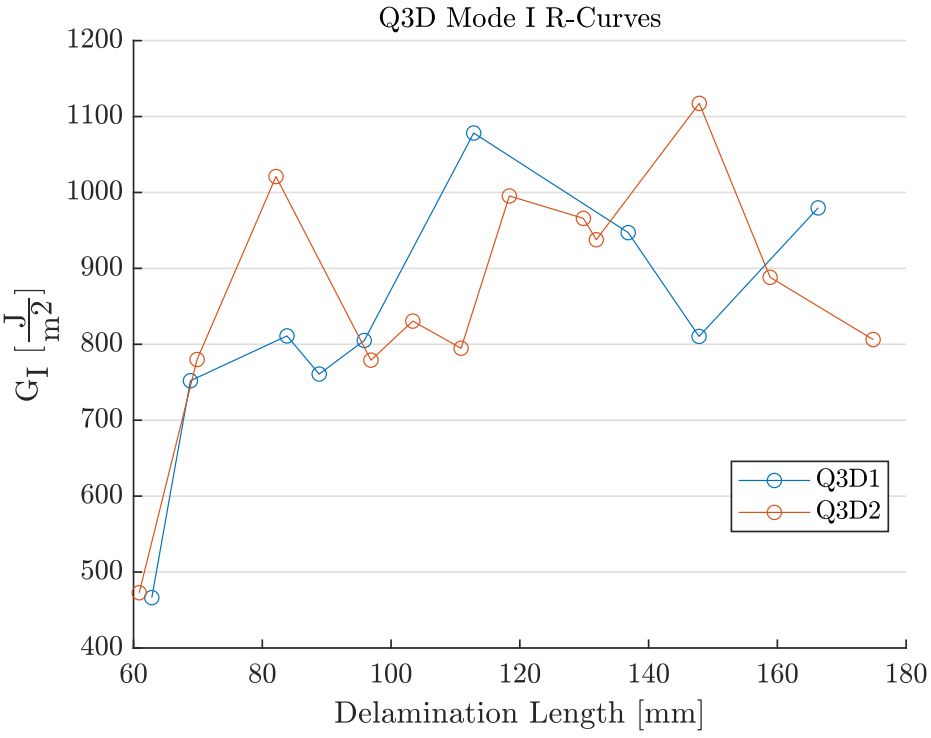

Figure A.3: Q3D mode I R-curves

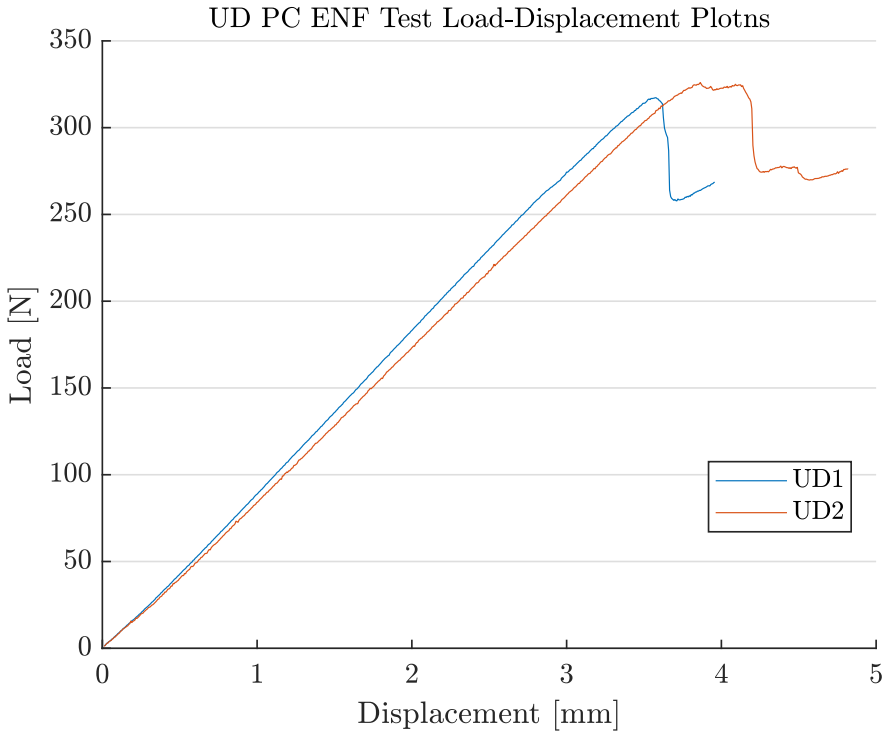

Figure A.4: UD mode II load-displacement plots

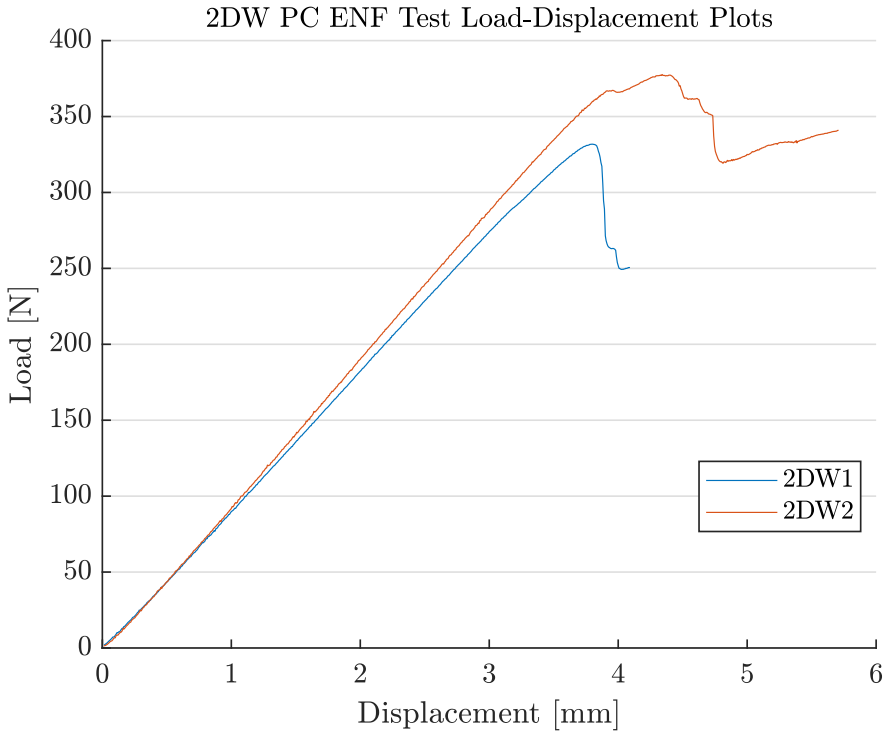

Figure A.5: 2DW mode II load-displacement plots

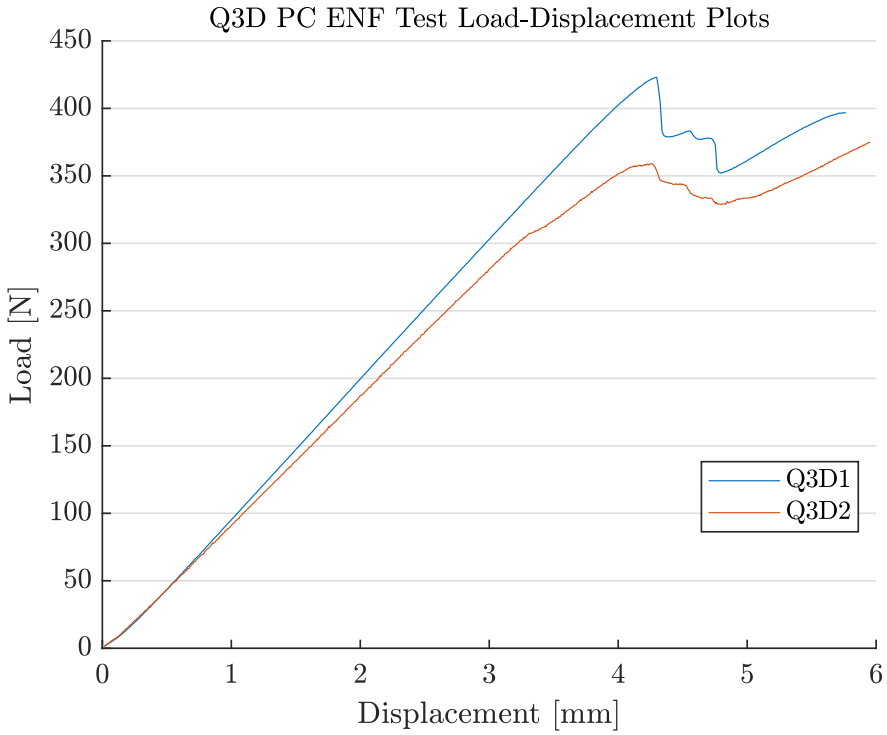

Figure A.6: Q3D mode II load-displacement plots

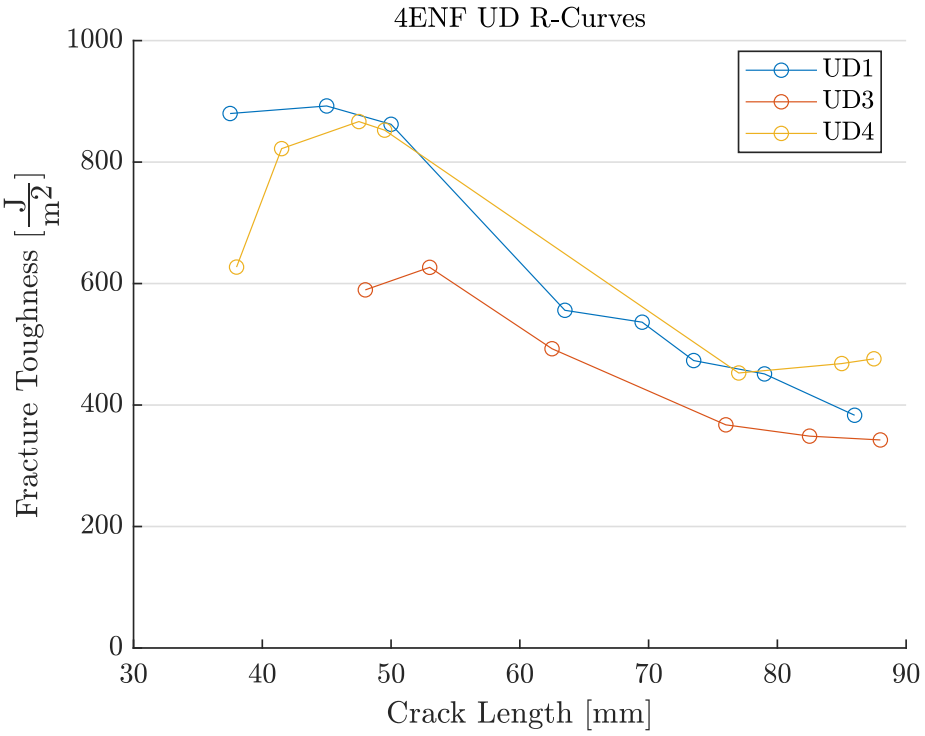

Figure A.7: UD mode II 4ENF R-curves

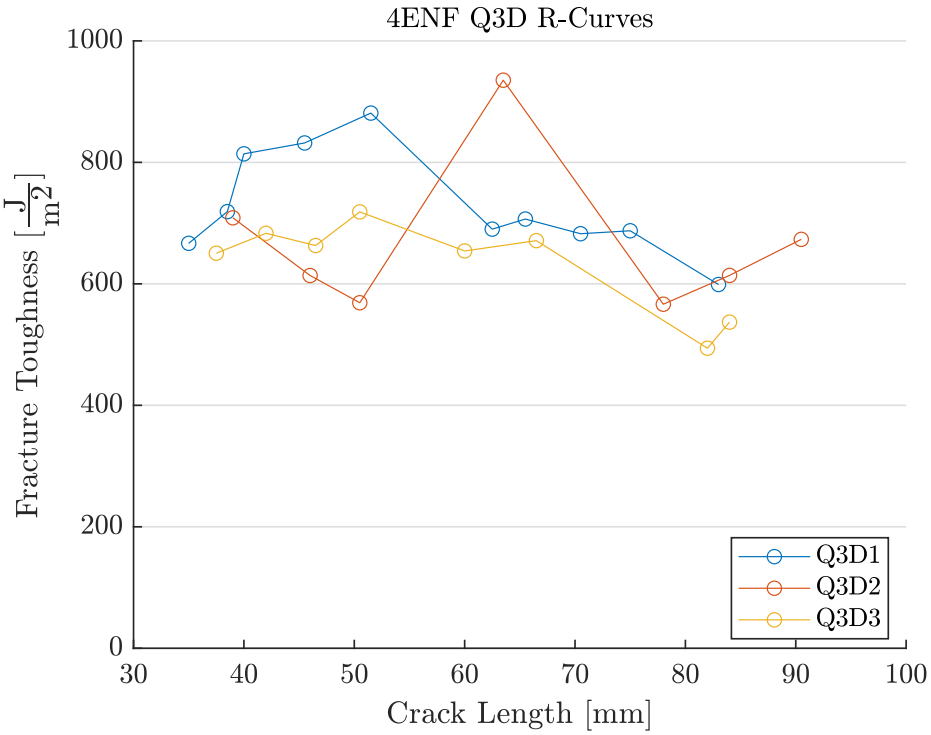

Figure A.8: Q3D mode II 4ENF R-curves

BIBLIOGRAPHY

BIBLIOGRAPHY

[1] X. Mao, "Mode I and II interlaminar fracture toughness simulation of unidirectional and quasi-three-dimensional composites," Master's thesis, Michigan State University, 2019.

[2] W. Zhou, *Peridynamic modeling and impact testing of dynamic damage, fracture, and failure process in fiber-reiforced composite materials.* PhD thesis, Michigan State University, 2018.

[3] ASTM International, "D5528-13 Standard Test Method for Mode I Interlaminar Fracture Toughness of Unidirectional Fiber-Reinforced Polymer Matrix Composites," standard, ASTM International, West Conshohocken, PA, 2013.

[4] ASTM International, "D7905/D7905M-19e1 Standard Test Method for Determination of the Mode II Interlaminar Fracture Toughness of Unidirectional Fiber-Reinforced Polymer Matrix Composites," standard, ASTM International, West Conshohocken, PA, 2019.

[5] R. H. Martin and B. D. Davidson, "Mode II fracture toughness evaluation using four point bend, end notched flexure test," *Plastics, Rubber and Composites*, vol. 28, pp. 401–406, aug 1999.

[6] D. Göktaş, W. R. Kennon, and P. Potluri, "Improvement of mode I interlaminar fracture toughness of stitched glass/epoxy composites," *Applied Composite Materials*, vol. 24, pp. 351–375, Nov. 2016.

[7] A. P. Mouritz, C. Baini, and I. Herzberg, "Mode I interlaminar fracture toughness properties of advanced textile fiberglass composites," *Composites Part A Applied Science and Manufacturing*, 1999.

[8] I. Gnaba, X. Legrnd, P. Wang, and D. Soulat, "Through-the-thickness reinforcement for composite structures: a review," *Journal of Inudstrial Textiles*, 2018.

[9] V. Dikshit, S. Bhudolia, and S. Joshi, "Multiscale polymer composites: a review of the interlaminar fracture toughness improvement," *Fibers*, vol. 5, p. 38, Oct. 2017.

[10] B. M'membe, S. Gannon, M. Yasaee, S. R. Hallett, and I. K. Partridge, "Mode II delamination resistance of composites reinforced with inclined z-pins," *Materials & Design*, vol. 94, pp. 565–572, Mar. 2016.

[11] A. P. Mouritz, M. K. Bannister, P. J. Falzon, and K. H. Leong, "Review of applications for advanced threee-dimensional fibre textile composites," *Composites Part A Applied Science and Manufacturing*, 1999.

[12] A. P. Mouritz, K. H. Leong, and I. Herszberg., "A review of the effect of stitching on the in-plane mechanical properties of fibre-reinforced polymer composites," *Composites Part A Applied Science and Manufacturing*, 1997.

[13] D. D. R. Cartié, M. Troulis, and I. K. Partridge, "Delamination of z-pinned carbon fibre reinforced laminates," *Composites Science and Technology*, vol. 66, pp. 855–861, May 2006.

[14] B. Zhang, G. Allegri, and S. R. Hallett, "An experimental investigation into multi-functional z-pinned composite laminates," *Materials & Design*, vol. 108, pp. 679–688, Oct. 2016.

[15] A. P. Mouritz, "Review of z-pinned composite laminates," *Composites Part A: Applied Science and Manufacturing*, vol. 38, pp. 2383–2397, Dec. 2007.

[16] A. P. Mouritz, "Compression properties of z-pinned composite laminates," *Composites Science and Technology*, vol. 67, pp. 3110–3120, Dec. 2007.

[17] A. Kerber, A. Gargano, K. Pingkarawat, and A. P. Mouritz, "Explosive blast damage resistance of three-dimensional textile composites," *Composites Part A: Applied Science and Manufacturing*, vol. 100, pp. 170–182, Sept. 2017.

[18] D. Liu, C.-Y. Lee, C.-F. Yen, C. Anderson, and G. Li, "Composite structure and method of making a composite structure," Mar. 2016.

[19] K. Rosario and D. Liu, "Assessment of quasi-three-dimensional composites - with discussions on fiber straining and weaving effectiveness," *Journal of Composite Materials*, 2010.

[20] D. Liu, K. Rosario, and S. Klann, "Behavior of quasi-three-dimensional woven composites," *American Society of Composites 2008*, 2008.

[21] H. Bayraktar, D. Ehrlich, J. Goering, and M. McClain, "3D woven composites for energy absorbing applications," *20th International Conference on Composite Materials*, 2015.

[22] Y. Zhao, M. Cao, W. P. Lum, V. B. C. Tan, and T. E. Tay, "Interlaminar fracture toughness of hybrid woven carbon-Dyneema composites," *Composites Part A: Applied Science and Manufacturing*, vol. 114, pp. 377–387, Nov. 2018.

[23] T. O'Brien, W. Johnston, and G. Toland, "Mode II interlaminar frafture toughness and fatigue characeterization of a graphite epoxy composite material," *NASA*, 2010.

[24] W.-X. Wang, M. Nakata, Y. Takao, and T. Matsubara, "Experimental investigation on test methods for mode II interlaminar fracture testing of carbon fiber reinforced

composites," *Composites Part A: Applied Science and Manufacturing*, vol. 40, pp. 1447–1455, sep 2009.

[25] ASTM International, "D3171-15 Standard Test Methods for Constituent Content of Composite Materials," standard, ASTM International, West Conshohocken, PA, 2010.

[26] A. Balakrishnan and M. C. Saha, "Tensile fracture and thermal conductivity characterization of toughened epoxy/CNT nanocomposites," *Materials Science and Engineering: A*, vol. 528, pp. 906–913, jan 2011.

[27] B. R. K. Blackman, A. J. Brunner, and J. G. Williams, "Mode II fracture testing of composites: a new look at an old problem," *Engineering Fracture Mechanics*, vol. 73, pp. 2443–2455, nov 2006.

[28] P. Davies, G. D. Sims, B. R. K. Blackman, A. J. Brunner, K. Kageyama, M. Hojo, K. Tanaka, G. Murri, C. Rousseau, B. Gieseke, and R. H. Martin, "Comparison of test configurations for determination of mode II interlaminar fracture toughness results from international collaborative test programme," *Plastics, Rubber and Composites*, vol. 28, pp. 432–437, Sept. 1999.

[29] C. Schuecker and B. D. Davidson, "Evaluation of the accuracy of the four-point bend end-notched flexure test for mode II delamination toughness determination," *Composites Science and Technology*, vol. 60, pp. 2137–2146, aug 2000.

[30] K. Kageyama, I. Kimpara, T. Suzuki, I. Ohsawa, M. Kanai, and H. Tsuno, "Effects of test conditions of mode II interlaminar fracture toughness of four-point ENF specimens," *Proceedings of the 1999 International Conference on Composite Materials*, 1999.

[31] P. Davies, P. Casari, and L. A. Carlsson, "Influence of fibre volume fraction on mode II interlaminar fracture toughness of glass/epoxy using the 4ENF specimen," *Composites Science and Technology*, vol. 65, pp. 295–300, feb 2005.

[32] G. Marannano, F. Parrinello, and A. Pasta, "Numerical and experimental analysis of the frictional effects on 4ENF delamination tests performed on unidirectional CFRP," *Procedia Engineering*, vol. 109, pp. 372–380, 2015.

[33] J. R. Reeder, K. Demarco, and K. S. Whitley, "The use of doubler reinforcement in delamination toughness testing," *Composites Part A: Applied Science and Manufacturing*, vol. 35, pp. 1337–1344, nov 2004.

[34] B. D. Davidson and X. Sun, "Effects of friction, geometry, and fixture compliance on the perceived toughness from three-and four-point bend end-notched flexure tests," *Journal of Reinforced Plastics and Composites*, vol. 24, pp. 1611–1628, jun 2005.

[35] G. C. Coppens and D. Liu, "Effects of through-thickness fiber geometry and snall angle on impact resistance," *Journal of Advanced Materials*, 2007.

[36] ASTM International, "D3039/D3039M-17 Standard Test Method for Tensile Properties of Polymer Matrix Composite Materials," standard, ASTM International, West Conshohocken, PA, 2017.

[37] ASTM International, "D7264/D7264M-15 Standard Test Method for Flexural Properties of Polymer Matrix Composite Materials," standard, ASTM International, West Conshohocken, PA, 2015.